Electronic Supplementary Information

Temperature and Isotope Effects in the Reaction of CH_3CHOO with Methanol

Wen Chao,[a] Yen-Hsiu Lin,[a,b] Cangtao Yin,[a] Wei-Hong Lin,[a] Kaito Takahashi,[a]* and Jim Jr-Min Lin[a,b]*

Table of Contents

Notations for the reaction rate coefficients in this work

rate coefficient	Reaction	Reaction order
k_{0s}	*syn*-CH_3CHOO when $[CH_3OH] = 0$	1
k_{1Hs}	*syn*-$CH_3CHOO+1CH_3OH$	2
k_{2Hs}	*syn*-$CH_3CHOO+2CH_3OH$	3
k_{1Ds}	*syn*-$CH_3CHOO+1CH_3OD$	2
k_{2Ds}	*syn*-$CH_3CHOO+2CH_3OD$	3
k_{0sd}	*syn*-CD_3CDOO when $[CH_3OH] = 0$	1
k_{1Hsd}	*syn*-$CD_3CDOO+1CH_3OH$	2
k_{2Hsd}	*syn*-$CD_3CDOO+2CH_3OH$	3
k_{0a}	*anti*-CH_3CHOO when $[CH_3OH] = 0$	1
k_{1Ha}	*anti*-$CH_3CHOO+1CH_3OH$	2

Table S1. Summary of the experimental conditions for the reaction *syn*-CH$_3$CHOO+2CH$_3$OH.

Exp#	[CH$_3$CHI$_2$] /10^{14} cm^{-3}	[CH$_3$CHOO]$_0$ /10^{11} cm^{-3}	P_{O2} /Torr	P_{total} /Torr	T /K	$I_{248\,nm}$ /mJ cm^{-2}	Isotopologue
1	2.06	3.41	11.3	250.2	299.3	1.70	CH$_3$OH
2	2.08	3.89	11.4	250.4	303.6	1.81	CH$_3$OH
3	1.95	3.84	11.4	250.2	323.5	1.74	CH$_3$OH
4	2.04	3.84	11.4	250.3	303.7	1.81	CH$_3$OH
5	1.97	4.25	11.3	249.6	298.1	1.70	CH$_3$OH
6	1.14	2.45	11.2	249.6	297.9	1.80	CH$_3$OH
7	2.33	5.03	11.2	249.6	298.0	1.75	CH$_3$OH
8	2.15	4.63	11.2	249.6	298.0	1.72	CH$_3$OH
9	2.30	4.28	11.7	249.9	283.3	1.84	CH$_3$OH
10	2.27	4.20	11.7	249.9	293.5	1.80	CH$_3$OH
11	2.26	4.04	11.7	249.9	303.6	1.79	CH$_3$OH
12	2.21	4.61	11.7	249.8	283.1	1.76	CH$_3$OH
13	2.22	4.24	11.5	250.0	273.0	1.80	CH$_3$OH
14	0.55	1.39	11.5	250.0	273.0	1.81	CH$_3$OH
15	1.12	2.37	11.5	249.9	273.0	1.77	CH$_3$OH
16	2.23	4.67	11.5	250.0	273.0	1.79	CH$_3$OH
17	0.48	2.07	11.5	250.0	323.6	3.53	CH$_3$OH
18	1.87	7.57	11.6	250.0	323.6	3.51	CH$_3$OH
19	0.95	3.87	11.6	250.0	323.6	3.46	CH$_3$OH
20	0.46	2.08	11.6	250.0	323.5	3.45	CH$_3$OH
21	1.08	2.50	12.3	50.5	298.6	1.75	CH$_3$OH
22	1.55	4.27	11	100.2	298.6	1.80	CH$_3$OH
23	1.51	3.21	10.9	249.8	298.6	1.77	CH$_3$OH
24	1.47	3.96	11.1	50.5	298.5	1.81	CH$_3$OH
25	1.98	4.14	11.4	250.1	298.4	1.71	CH$_3$OH
26	1.82	2.54	11.5	756.3	298.5	1.67	CH$_3$OH
27	1.84	3.19	11.3	499.3	298.5	1.53	CH$_3$OH
28	2.58	5.67	14	30.3	298.6	1.86	CH$_3$OH
29	1.94	5.04	11.6	100.3	298.6	1.86	CH$_3$OH
30	1.93	4.02	11.3	250.0	298.6	1.81	CH$_3$OH
31	1.76	4.07	11.3	250.0	323.7	1.83	CH$_3$OH
32	1.86	5.42	12.4	30.4	323.6	1.89	CH$_3$OH
33	1.80	4.76	11.7	100.4	323.5	1.76	CH$_3$OH
34	0.82	4.19	11.2	250.2	313.6	3.56	CH$_3$OH

35	0.42	2.23	11.2	250.3	313.6	3.50	CH_3OH
36	1.65	7.46	11.2	250.3	313.6	3.42	CH_3OH
37	0.40	2.04	11.2	250.3	323.6	3.41	CH_3OH
38	1.60	7.74	11.2	250.3	323.6	3.37	CH_3OH
39	0.79	4.14	11.2	250.3	323.6	3.41	CH_3OH
40	1.73	4.30	11.0	250.2	323.6	1.81	CH_3OD
41	1.75	4.27	11.0	250.0	313.4	1.76	CH_3OD
42	1.68	3.79	10.9	250.2	313.3	1.58	CH_3OD
43	1.93	4.12	10.9	250.2	293.2	1.83	CH_3OD
44	2.05	4.21	10.9	250.1	273.0	1.82	CH_3OD
45	1.95	4.58	10.9	250.1	283.1	1.79	CH_3OD
46	1.77	4.28	10.9	250.1	303.3	1.82	CH_3OD
47 [a]	0.71 [b]	2.84 [b]	10.9	250.2	323.7	2.68	CH_3OH
48 [a]	0.74 [b]	2.22 [b]	10.9	250.2	298.6	2.69	CH_3OH

[a] The reaction syn-CD_3CDOO+$2CH_3OH$.

[b] By assuming the same UV absorption cross section as the normal isotopologues ($\sigma_{CH3CHI2}$ = 3.61×10^{-18} cm^{-2} at 296 nm;[1] $\sigma_{syn\text{-}CH3CHOO}$ = 1.19×10^{-17} cm^{-2} at 340 nm^2).

Table S2. Summary of the quadratic fit with and without the first order term for *syn*-CH$_3$CHOO reaction with CH$_3$OH vapor. The negative values and the values that are smaller than their fitting error are marked in red.

Exp #	P_{total} /Torr	T /K	with k_{1Hs} term k_{0s} /s^{-1}	k_{1Hs} /10^{-16} cm^3 s^{-1}	k_{2Hs} /10^{-32} cm^6 s^{-1}	without k_{1Hs} term k_{0s} /s^{-1}	k_{2Hs} /10^{-32} cm^6 s^{-1}	[CH$_3$OH] /10^{16} cm^{-3}
1	250.2	299.3	363.6 ± 43.6 [a]	6.3 ± 11.2	7.2 ± 0.4	384.4 ± 22.1	7.4 ± 0.1	1.7 - 33.8
2	250.4	303.6	450.5 ± 18.6	8.8 ± 4.7	5.1 ± 0.2	483.3 ± 7.3	5.5 ± 0.0	2.5 - 22.2
3	250.2	323.5	875.4 ± 22.8	19.9 ± 4.7	0.8 ± 0.2	961.1 ± 15.7	1.5 ± 0.1	2.4 – 28.0
4	250.3	303.7	433.1 ± 22.7	11.6 ± 5.8	4.8 ± 0.2	471.8 ± 12.6	5.2 ± 0.1	1.6 - 29.6
5	249.6	298.1	409.7 ± 47.9	0.7 ± 12.7	8.4 ± 0.5	411.9 ± 23.2	8.4 ± 0.1	1.7 - 30.7
6	249.6	297.9	300.9 ± 60.2	25.1 ± 16.4	7.1 ± 0.6	381.1 ± 30.9	8.0 ± 0.2	1.7 - 30.5
7	249.6	298.0	379.8 ± 31.0	23.6 ± 8.1	7.0 ± 0.3	458.0 ± 18.3	7.9 ± 0.1	1.7 - 30.6
8	249.6	298.0	376.9 ± 27.0	12.4 ± 7.2	7.3 ± 0.3	417.4 ± 14.2	7.8 ± 0.1	1.7 - 30.4
9	249.9	283.3	259.6 ± 45.9	17.9 ± 18.6	24.9 ± 1.2	299.7 ± 19.2	26.1 ± 0.4	1.4 - 17.5
10	249.9	293.5	356.7 ± 47.0	3.9 ± 13.4	11.0 ± 0.6	368.7 ± 21.7	11.2 ± 0.2	1.8 - 27.6
11	249.9	303.6	466.6 ± 23.9	2.9 ± 5.9	5.3 ± 0.2	476.7 ± 11.8	5.4 ± 0.1	1.7 - 30.6
12	249.8	283.1	177.6 ± 47.8	60.2 ± 19.4	21.2 ± 1.2	312.2 ± 24.6	24.9 ± 0.4	1.5 - 17.5
13	250.0	273.0	192.4 ± 76.8	59.0 ± 40.4	55.5 ± 4	296.1 ± 30.8	61.1 ± 1.1	1.4 - 10.4
14	250.0	273.0	-96.8 ± 221.9	167.3 ± 149	45.9 ± 19.7	140.1 ± 69.6	67.4 ± 4.7	1.5 - 7.2
15	249.9	273.0	77.5 ± 203.3	70.1 ± 108.7	54.0 ± 10.7	198.7 ± 75.5	60.7 ± 2.8	1.5 - 10.6
16	250.0	273.0	374.9 ± 63.6	-59.3 ± 32.7	71.0 ± 3.2	268.1 ± 26.1	65.4 ± 0.9	1.5 - 10.5
17	250.0	323.6	990.0 ± 40.9	1.1 ± 7.3	1.4 ± 0.2	995.2 ± 19.5	1.4 ± 0.1	2.2 - 30.9
18	250.0	323.6	1011.9 ± 14.5	12.0 ± 2.6	1.1 ± 0.1	1070.7 ± 10.9	1.4 ± 0.0	2.2 - 31.6
19	250.0	323.6	973.1 ± 14.1	4.1 ± 2.5	1.3 ± 0.1	993.5 ± 7.3	1.4 ± 0.0	2.2 - 31.8
20	250.0	323.5	955.5 ± 44.5	-3.7 ± 7.8	1.6 ± 0.3	937.1 ± 21.3	1.4 ± 0.1	2.2 - 31.6
21	50.5	298.6	308.4 ± 29.1	7.6 ± 7.4	6.0 ± 0.3	334.9 ± 13.8	6.3 ± 0.1	1.6 - 21.1
22	100.2	298.6	341.5 ± 66.3	15.8 ± 16.2	6.4 ± 0.7	398.1 ± 31.6	7.0 ± 0.2	1.7 – 22.0
23	249.8	298.6	366.9 ± 9.2	6.7 ± 2.9	7.6 ± 0.1	385.9 ± 4.7	8.0 ± 0.1	1.6 - 21.7
24	50.5	298.5	379.5 ± 30.5	-5.3 ± 7.6	6.7 ± 0.3	360.6 ± 13.9	6.5 ± 0.1	1.7 - 21.3
25	250.1	298.4	416.5 ± 42.5	-0.4 ± 10.3	8.0 ± 0.5	415.1 ± 18.2	8.0 ± 0.1	2.5 - 23.6
26	756.3	298.5	232.2 ± 101.3	44.8 ± 17.3	6.5 ± 0.6	467.5 ± 54.7	8.0 ± 0.2	2.7 - 25.5
27	499.3	298.5	321.7 ± 64.0	19.8 ± 11.2	7.4 ± 0.4	422.8 ± 30.7	8.1 ± 0.1	2.6 - 24.8
28	30.3	298.6	376.6 ± 106.8	13.8 ± 14.2	4.2 ± 0.4	464.5 ± 57.5	4.6 ± 0.1	2.3 - 35.8
29	100.3	298.6	408.8 ± 27.9	4.5 ± 5.9	7.2 ± 0.2	427.5 ± 12.8	7.4 ± 0.1	1.6 - 22.4
30	250.0	298.6	392.0 ± 20.3	6.6 ± 5.5	7.6 ± 0.3	414.0 ± 8.5	7.9 ± 0.1	2.5 - 20.1
31	250.0	323.7	926.9 ± 27.4	18.5 ± 4.5	0.9 ± 0.1	1025.4 ± 22.6	1.4 ± 0.1	3.2 - 30.9

Exp #	P_{total} /Torr	T /K	k_{0s} /s^{-1}	k_{1Ds} /10^{-16} cm^3 s^{-1}	k_{2Ds} /10^{-32} cm^6 s^{-1}	k_{0s} /s^{-1}	k_{2Ds} /10^{-32} cm^6 s^{-1}	[CH$_3$OD] /10^{16} cm^{-3}
32	30.4	323.6	788.2 ± 36.0	12.4 ± 4.3	0.7 ± 0.1	874.2 ± 27.6	1.0 ± 0.0	2.3 - 37.9
33	100.4	323.5	884.4 ± 21.3	11.8 ± 3.1	1.0 ± 0.1	955.3 ± 16.7	1.4 ± 0.0	3.1 - 29.6
34	250.2	313.6	676.5 ± 17.6	3.1 ± 3.1	2.5 ± 0.1	691.9 ± 8.2	2.6 ± 0.0	3.0 - 30.1
35	250.3	313.6	703.8 ± 26.5	-7.8 ± 4.7	2.9 ± 0.2	664.3 ± 13.4	2.7 ± 0.0	3.0 - 30.2
36	250.3	313.6	776.3 ± 16.5	9.0 ± 2.9	2.4 ± 0.1	821.8 ± 10.6	2.6 ± 0.0	3.0 - 30.2
37	250.3	323.6	985.1 ± 29.6	1.8 ± 5.0	1.4 ± 0.2	994.8 ± 13.3	1.4 ± 0.0	2.9 - 29.3
38	250.3	323.6	1077.9 ± 19.8	8 ± 3.3	1.1 ± 0.1	1120.4 ± 11.4	1.4 ± 0.0	2.9 - 29.3
39	250.3	323.6	933.1 ± 34.0	14.9 ± 5.7	1.0 ± 0.2	1011.0 ± 20.0	1.4 ± 0.1	2.9 - 29.3

[a] ±1σ of the fitting error.

Table S3. Summary of the quadratic fit with and without the first order term for *syn*-CH$_3$CHOO reaction with CH$_3$OD vapor. The negative values and the values that are smaller than their fitting error are marked in red.

			with k_{1Ds} term			without k_{1Ds} term		
	P_{total}	T	k_{0s}	k_{1Ds}	k_{2Ds}	k_{0s}	k_{2Ds}	[CH$_3$OD]
Exp #	/Torr	/K	/s^{-1}	/10^{-16} cm^3 s^{-1}	/10^{-32} cm^6 s^{-1}	/s^{-1}	/10^{-32} cm^6 s^{-1}	/10^{16} cm^{-3}
40	250.2	323.6	935.7 ± 28.5 [a]	12.5 ± 5.3	0.2 ± 0.2	994.1 ± 17.7	0.7 ± 0.0	2.6 - 26.3
41	250.0	313.4	670.1 ± 17.3	3.3 ± 3.4	0.9 ± 0.1	684.4 ± 8.7	1.0 ± 0.0	2.2 - 27.1
42	250.2	313.3	622.2 ± 15.5	4.3 ± 3.1	1.0 ± 0.1	641.5 ± 7.5	1.1 ± 0.0	2.2 - 26.3
43	250.2	293.2	376.7 ± 38.6	-0.2 ± 7.6	4.7 ± 0.3	375.8 ± 15.8	4.7 ± 0.1	2.5 - 25.6
44	250.1	273.0	379.2 ± 120.3	-42.6 ± 36.3	29.2 ± 2.4	244.8 ± 36.8	26.4 ± 0.4	2.7 - 12.3
45	250.1	283.1	266.8 ± 87.9	9.8 ± 21.2	10.2 ± 1	304.4 ± 32.7	10.7 ± 0.2	2.5 - 17.8
46	250.1	303.3	478.3 ± 22.5	1.8 ± 4.0	2.1 ± 0.1	487.4 ± 9.2	2.1 ± 0.0	2.4 - 27.6

[a] ± 1σ of the fitting error.

Table S4. Summary of the quadratic fit with and without the first order term for *syn*-CD$_3$CDOO reaction with CH$_3$OH vapor. The negative values and the values that are smaller than their fitting error are marked in red.

			with k_{1Hsd} term			without k_{1Hsd} term		
	P_{total}	T	k_{0sd}	k_{1Hsd}	k_{2Hsd}	k_{0sd}	k_{2Hsd}	[CH$_3$OH]
Exp #	/Torr	/K	/s^{-1}	/10^{-16} cm^3 s^{-1}	/10^{-32} cm^6 s^{-1}	/s^{-1}	/10^{-32} cm^6 s^{-1}	/10^{16} cm^{-3}
47	250.2	323.7	381.8 ± 12.0 [a]	0.8 ± 2.7	1.7 ± 0.1	385.1 ± 5.1	1.7 ± 0.0	2.2 - 27.4
48	250.2	298.6	184.6 ± 41.3	8.5 ± 12.2	9.1 ± 0.6	210.8 ± 16.9	9.5 ± 0.2	2.4 - 20.1

[a] ± 1σ of the fitting error.
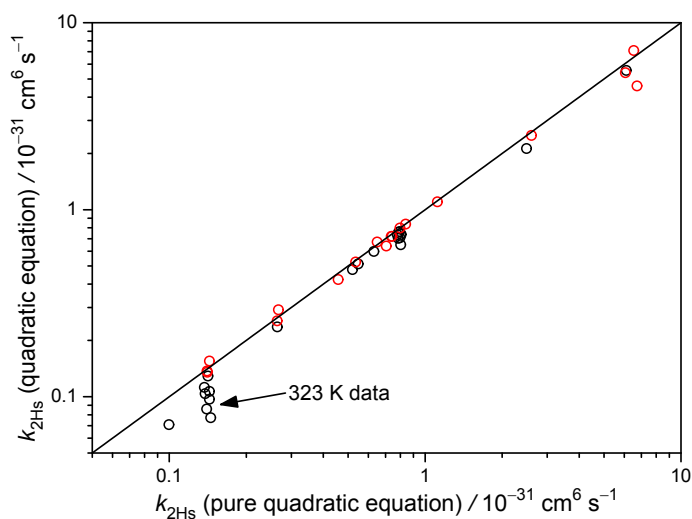
Fig. S1. Comparison between the k_{2Hs} values obtained from the quadratic fit with and without considering the first order term. The cases of which the k_{1Hs} value is negative or smaller than its fitting error are marked as red circles. The deviation from the one-to-one line is larger at 323 K because the quadratic feature is less clear at high temperature.

Table S5. Summary of the experimental conditions for the reaction *anti*-$CH_3CHOO+CH_3OH$.

Exp #	$[CH_3CHI_2]$	P_{O2}	P_{total}	T	$I_{248\ nm}$	k_{0a}	k_{1Ha}
	$/10^{14}\ cm^{-3}$	/Torr	/Torr	/K	/mJ cm^{-2}	/s^{-1}	$/10^{-12}\ cm^3\ s^{-1}$
49	2.05 [a]	11.3	100.4	297.8	2.01	1062.6 ± 51.0 [b]	4.1 ± 0.0 [b]
50	1.95	11.2	100.6	297.4	1.67	979.6 ± 138.2	4.1 ± 0.1
51	2.20	11.8	100.5	298.3	1.91	965.6 ± 138.8	3.8 ± 0.1
52	2.28	11.8	100.3	298.2	1.48	1147.4 ± 129.0	4.0 ± 0.1
53	2.14	11.4	100.5	298.1	1.48	965.9 ± 151.9	4.0 ± 0.1
54	2.23	11.7	100.2	298.1	1.68	1123.9 ± 77.2	4.1 ± 0.1
55	2.09	11.7	100.4	297.5	1.53	1102.2 ± 129.7	4.1 ± 0.1
56	2.05	11.4	250.7	297.9	1.91	1218.6 ± 179.8	4.7 ± 0.1
57	2.01	11.2	250.6	298.3	1.48	1020.4 ± 263.0	4.8 ± 0.2
58	2.19	11.4	250.7	298.0	1.68	970.3 ± 103.2	5.0 ± 0.1
59	2.10	11.3	250.6	298.1	1.68	872.5 ± 105.8	5.1 ± 0.1
60	2.06	11.4	250.6	298.2	1.68	861.7 ± 95.3	4.9 ± 0.1
61	2.16	11.3	250.8	298.1	1.76	955.0 ± 103.4	4.6 ± 0.1
62	1.59	11.4	250.7	298.1	1.79	622.0 ± 220.5	5.3 ± 0.2
63	2.01	11.3	501.4	297.4	1.53	777.8 ± 133.1	5.6 ± 0.1
64	2.00	11.3	501.4	297.4	1.53	703.8 ± 81.3	5.8 ± 0.1
65	2.14	11.4	250.7	287.8	1.68	1130.8 ± 198.3	5.7 ± 0.2
66	2.22	11.4	250.6	288.0	1.68	905.7 ± 19.5	5.7 ± 0.0
67	1.61	11.4	250.8	315.1	1.79	616.8 ± 86.5	3.7 ± 0.1
68	1.57	11.4	250.6	315.1	1.79	478.5 ± 42.5	3.7 ± 0.0

[a] deduced with $\sigma_{CH3CHI2}$ = 3.61x10^{18} cm^{-2} at 296 nm.[1]

[b] ±1σ of the fitting error.

Error estimation

The errors of the reaction rate coefficients were estimated by considering mainly (i) the uncertainties in the methanol concentrations and (ii) the experimental stability. Assuming that all these uncertainties are uncorrelated, we estimated the error bar as below.

The UV absorption of methanol was recorded in a glass cell at wavelengths 190 – 220 nm. The concentration of methanol was derived by using the Beer-Lambert law. The main uncertainty comes from the literature absolute cross section of methanol, which is 5%.[3] The relative error of the absorbance measurement is 2%, mainly due to the baseline drifting. The effective length of the absorption cell is 90.3±0.1 cm.

The [CH_3OH] in the reactor was derived by taking into account the dilution factor of the flow mixing, the changes of pressures and temperatures between the glass cell and the reactor. All the flows were controlled by mass flow controllers (Brooks, 5850 or 5850E). The error of the flow dilution is about 1.4%. The temperature of the glass cell and the reactor were monitored by a temperature sensor (Rotronic, HC2-S, ±0.1 K at 10-30 °C) and three resistance temperature detectors (RTD, omega, ±0.5 K after calibration) located at the middle and two ends of the reactor. All the pressures were measured by diaphragm gauges (INFICON, ±0.2 % of reading). Since the errors of the temperature and pressure measurements are small, compared to the error of the flow dilution, the error for [CH_3OH] was estimated to be $[(5\%)^2 + (2\%)^2 + (1.4\%)^2]^{0.5} = 5.6\%$ (consider the relative uncertainties in the cross section, absorbance measurement, and flow dilution, respectively).

The experimental stability may show up in the scatter of the rate coefficients ($k_{2Hs}/k_{2Ds}/k_{2Hsd}$ values) measured under similar experimental conditions (*i.e.* at the same T and P) or the error of the fitting process (shown in Tables S2-S5). We chose the standard deviation of the former (5% for k_{2Hs}) to present the stability error because it is usually larger than that of the latter.

For the reaction of *syn*-CH_3CHOO+2CH_3OH, we estimated the final error of k_{2Hs} to be $[(2\times5.6\%)^2 + (5\%)^2]^{0.5} = 12\%$ (consider the relative uncertainties in [CH_3OH] and the stability of the k_{2Hs} values, respectively). Based on similar discussion, for the reaction of *anti*-CH_3CHOO+CH_3OH, the final error of k_{1Ha} is estimated to be $[5.6\%^2 + 8\%^2]^{0.5} = 10\%$. Since the error of the activation energy only depends on the relative values of the rate coefficients, we used the fitting error to represent the error bar of the activation energy.

Kinetic analysis for the reaction *anti*-CH₃CHOO+CH₃OH

Both *anti*- and *syn*-CH₃CHOO were generated in the reactor by the UV photolysis of 1,1-diiodoethane/O₂ mixture.[4,5] The absorption signals of both conformers were monitored in real time at 365 nm, where *anti*-CH₃CHOO has stronger absorption signal. Typical time traces were shown in Figure S2.
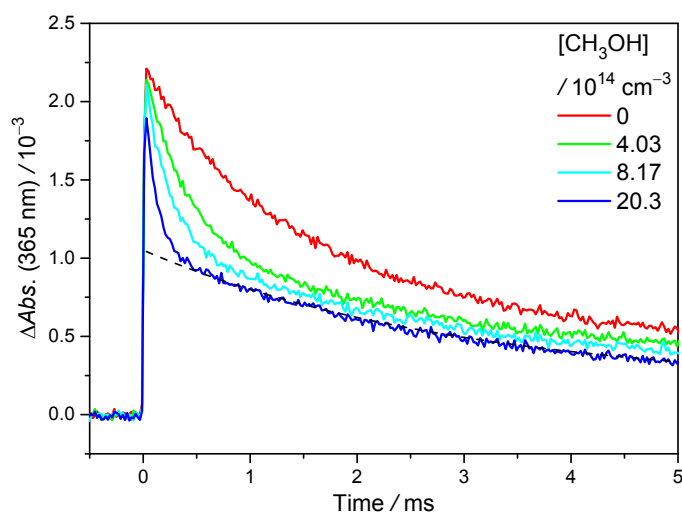

Fig. S2. Typical time traces of CH₃CHOO absorption signal at 365 nm under different [CH₃OH] at 298 K and 250 Torr (Exp#52). The photolysis laser sets the time zero. In the presence of CH₃OH, the time traces show a fast decay and a slow decay, which are assigned to *anti*-CH₃CHOO and *syn*-CH₃CHOO, respectively. The dashed line is the exponential fit to the slow decay of the blue line.

In Figure S2, the time traces of [CH₃OH] > 0 show a fast decay (<1 ms) and a slow decay (up to 5 ms). Base on the fact that *anti*-CH₃CHOO reacts with CH₃OH faster than *syn*-CH₃CHOO does, the fast decay was assigned to *anti*-CH₃CHOO and the slow decay to *syn*-CH₃CHOO.[5] The highest [CH₃OH] used in this experiment was about 2×10^{15} cm⁻³, which has negligible effect on the decay lifetime of *syn*-CH₃CHOO. The signals of *anti*-CH₃CHOO under various [CH₃OH] were obtained by subtracting the signal of *syn*-CH₃CHOO at the highest [CH₃OH] and were fitted by an exponential function.
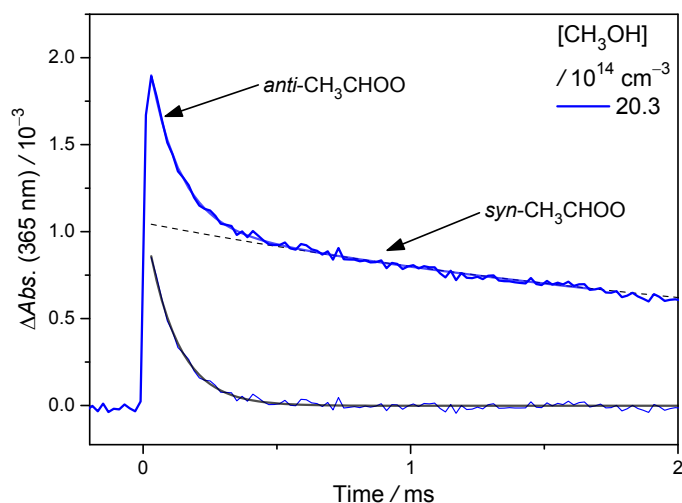
Fig. S3. The partition of the signals of *anti-* and *syn-*CH₃CHOO probed at 365 nm. Dashed line is the exponential fit to the slow decay of the time trace. The signal of *anti-*CH₃CHOO was obtained by subtracting the fitted exponential function from the raw data. The black line is the exponential fit to the "net" fast decay trace.

Figure S3 shows the separation of the signal of *anti-*CH₃CHOO from the signal of *syn-*CH₃CHOO. The net fast decay trace was fitted by an exponential function to yield the observed rate coefficient, $k_{obs(anti)}$. The experiments were carried out under 288-315 K and 100-501 Torr. All the experimental conditions and the fitting results were summarized in Table S5. As shown in Figure S4, the $k_{obs(anti)}$ showed good linearity under all studied conditions. We used the following equation to analysis the kinetics of *anti-*CH₃CHOO reaction with methanol.

$$-\frac{\mathrm{d}[anti\text{-}\mathrm{CH_3CHOO}]}{\mathrm{dt}} = (k_{0a} + k_{1Ha}[\mathrm{CH_3OH}])[anti\text{-}\mathrm{CH_3CHOO}]$$

$$= k_{obs(anti)}[anti\text{-}\mathrm{CH_3CHOO}]$$

Where k_{0a} denotes the background decay rate of *anti-*CH₃CHOO when [CH₃OH] = 0 and k_{1Ha} denotes the bimolecular rate coefficient.
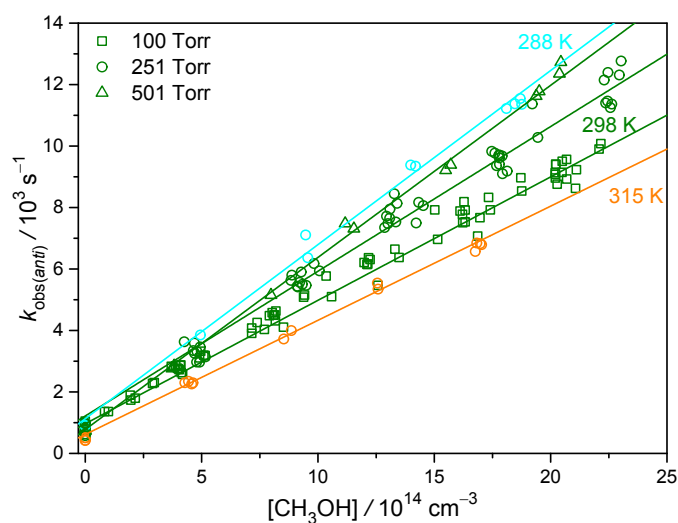
Fig. S4. Plot of the observed decay rate coefficient of *anti*-CH$_3$CHOO as a function of [CH$_3$OH] under 288, 298 and 315 K and 251 Torr (exp # 56-62 and 65-68). At 298K, experiments were also carries out under 100 and 501 Torr (exp # 49-55, 63 and 64). The $k_{obs(anti)}$ shows a linear dependence on [CH$_3$OH]. Solid lines are the linear fit. The reaction rate between *anti*-CH$_3$CHOO and CH$_3$OH is faster at lower temperature, showing a negative temperature effect.

Figure S 5 shows the Arrhenius plot of k_{1Ha}. We found that k_{1Ha} has a weak negative temperature dependence with an activation energy $E_a = -(2.8\pm0.3)$ kcal mol^{-1}, which is close to the calculated transition state energy (-4.87 kcal mol^{-1}). The bimolecular rate coefficients was determined to be $k_{1Ha} = (4.9\pm0.5)\times10^{-12}$ cm^3 s^{-1} at 250 Torr and 298 K. Theory overestimated the absolute value of the rate coefficient about a factor of 2. The potential energy surface of the reaction *anti*-CH$_3$CHOO+1CH$_3$OH was shown in Figure S6. We found two reaction pathways, differing from the orientation of the methyl group of CH$_3$OH. The transition state energy is lower than the reactants due to the strong interaction of *anti*-CH$_3$CHOO with CH$_3$OH.[6] The methoxymethyl hydroperoxide has been predicted as the product by theory.
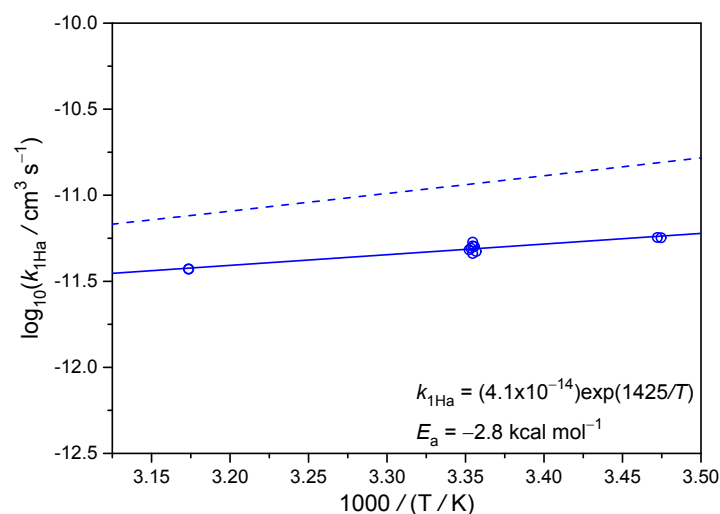
Fig. S5. Arrhenius plot of the reaction *anti*-CH₃CHOO+CH₃OH (Exp# 56-62,65-68) at 251 Torr. The k_{1Ha} shows a good linearity for T = 288-315 K with a negative temperature effect. The solid line is linear regression. The dashed line presents the calculated rate coefficients.
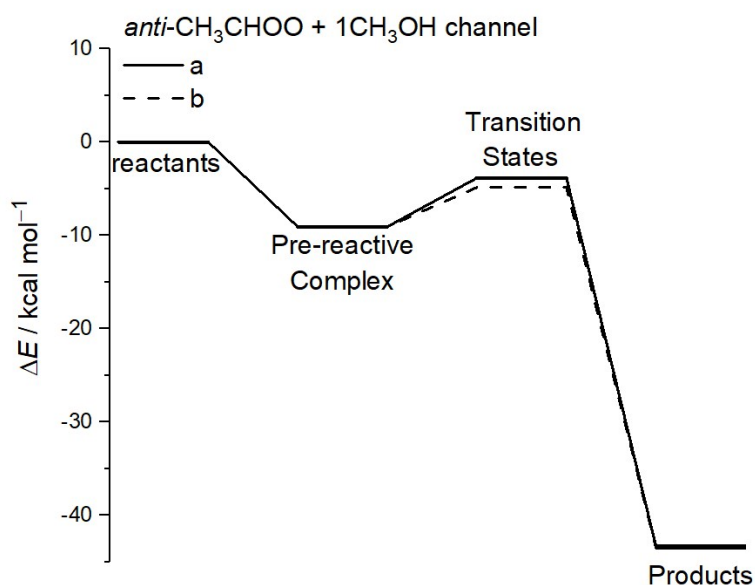

Fig. S6. Potential energy diagram for the reaction *anti*-CH₃CHOO+1CH₃OH. The solid and dashed lines represent difference reaction pathway (a, b). Energies were calculated at QCISD(T)/CBS//B3LYP/6-311+G(2d,2p) and vibrational zero-point energy corrections at B3LYP/6-311+G(2d,2p).

Pressure dependence for the reactions of CH_3OH with *anti-* and *syn-*CH_3CHOO
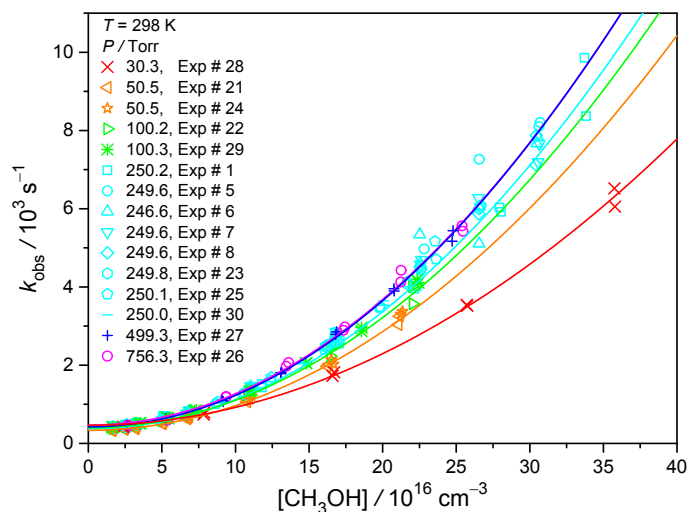

Fig. S7. Plot of the k_{obs} of *syn-*CH_3CHOO as a function of $[CH_3OH]$ at 30-756 Torr and 298 K (Exp #1, 5-8, 21-30). The observed decay rate coefficients show quadratic dependences on $[CH_3OH]$. The solid lines are pure quadratic equation fit.

The plot of k_{obs} as a function of $[CH_3OH]$ for the reaction *syn-*$CH_3CHOO+2CH_3OH$ at 30-756 Torr is shown in Figure S7. Figure S8 shows k_{2Hs} and k_{1Ha} as functions of the total pressure. We observed that k_{2H} increases with the total pressure for $P < 100$ Torr and reaches an asymptote near 250 Torr.

Under the low pressure conditions (<100Torr), methanol replaced more than 10% of the buffer gas (N_2) when we scanned $[CH_3OH]$. Since CH_3OH has a permanent dipole moment and a few low-frequency vibrational modes, the energy transfer efficiency between *syn-*CH_3CHOO and CH_3OH could be significantly better than the case of N_2; therefore, the reaction environment changes dramatically when scanning $[CH_3OH]$, resulting in an uncertainty of the observed pressure effect. Thus, we should consider the error bar of the pressure dependence is larger at $P < 100$ Torr.
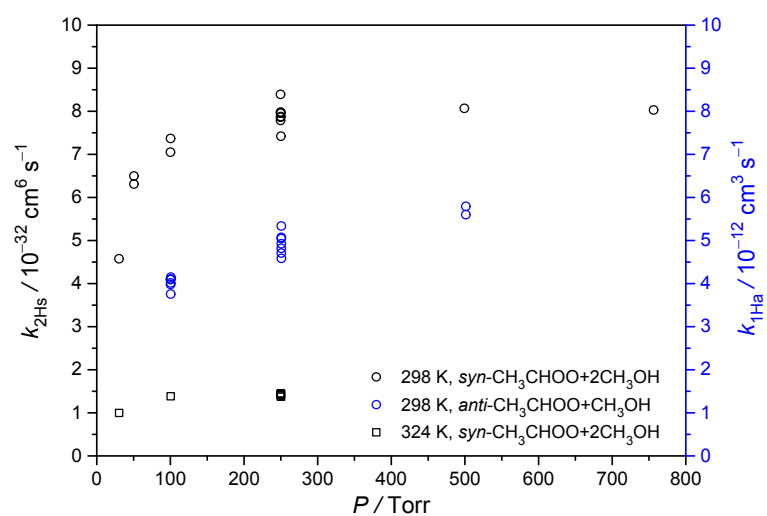
Fig. S8. The pressure dependence of the rate coefficients of the reaction *syn*-CH$_3$CHOO+2CH$_3$OH (left axis) at 298 K (black circle, Exp #1, 5-8, 21-30) and at 324K (black square, Exp # 3, 17-20, 31-33, 37-39), and the reaction *anti*-CH$_3$CHOO+CH$_3$OH (right axis, blue circle, Exp #56-68). No significant pressure effect was observed for the reaction *syn*-CH$_3$CHOO+2CH$_3$OH at 250-756 Torr while k_{1Ha} increases very slightly for $P \geq 250$ Torr.
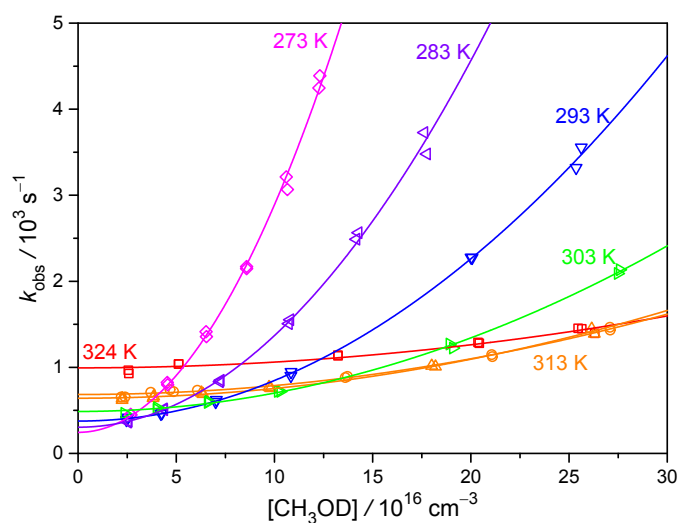
Fig. S9. Plot of k_{obs} of *syn*-CH$_3$CHOO as a function of [CH$_3$OD] at 273-324 K and 250 Torr (Exp# 40-46). The observed decay rate coefficient shows a quadratic dependence on [CH$_3$OD]. The solid lines are pure quadratic fit. Similar to the reaction *syn*-CH$_3$CHOO+2CH$_3$OH, a negative temperature dependence was observed.
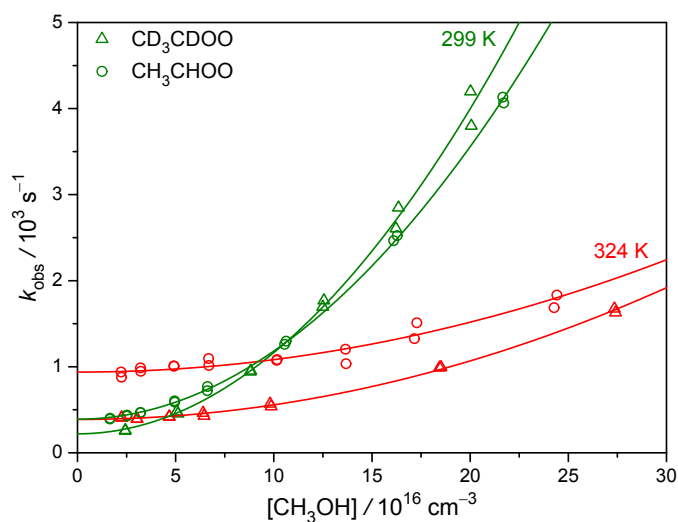

Fig. S10. Plot of k_{obs} of *syn*-CD$_3$CDOO and *syn*-CH$_3$CHOO as a function of [CH$_3$OH] at 299-324 K and 250 Torr (Exp# 20,23,47,48). The solid lines are pure quadratic fit. Notably, k_{0sd} (*syn*-CD$_3$CDOO) is smaller than k_{0s} (*syn*-CH$_3$CHOO) at the same temperature, especially at 324 K, consistent with the isotope effect of the thermal decomposition of *syn*-CH$_3$CHOO.[7,8]

Synthesis of CD$_3$CDI$_2$

The precursor, CD$_3$CDI$_2$, was synthesized by following a reported method with a few modifications.[9] 20 gram of hydrazine monohydrate (H$_2$NNH$_2$•H$_2$O, Wako, >97%) was refluxed 30 min to remove water with the opened end of the condenser connected to a drying tube. Then, 10 g of acetaldehyde-d4 (CD$_3$COD, CDN, >99.5%) was slowly added in hydrazine (water bath, >1hr) to get acetaldehyde hydrazone, (CD$_3$)CD=NH$_2$.

The solution in the flask was split and extracted by either ethyl ether or dichloromethane. We found that the efficiency to extract hydrazone by ethyl ether is low and we lost more than half of the products in this step; on the other hand, we succeeded to extract the hydrazine by using dichloromethane. Then, the solution was washed by saturated NaCl aqueous solution and was dried with MgSO$_4$. Finally, dichloromethane was removed by immersing the container in warm water bath (~ 45 °C).

The saturated solution of iodine in ether was added into the solution of hydrazone in ether and tetramethyl amine (TEA). The reaction is instantaneous and can be judged by the cessation of evolution of nitrogen gas and the persistence of iodine color. Due to the iodine salt formation, a 250 mL bottle was used to make the stir bar stir smoothly. After the reaction completed, the solution was extracted by ether and washed consecutively with 5% Na$_2$S$_2$O$_3$ (quenching iodine), 3M HCl (quenching TEA), 5 % Na$_2$CO$_3$ (neutralizing HCl), and saturated NaCl aqueous solution (removing water). Ethyl ether was removed after drying with MgSO$_{4(s)}$. The whole process mentioned above should be carefully done in a light-avoiding condition to prevent the photolysis of iodine.

The final yield of CD$_3$CDI$_2$ was very low because of the step extracting hydrazone with ethyl ether. We did not have enough amounts of CD$_3$CDI$_2$ to check the purity. Based on the facts that (1) we used acetaldehyde-d4 as the starting material, (2) the UV absorption signal in the Criegee intermediate experiment shows a fast and a slow decay in the presence of methanol, and (3) the background decay rate (k_{0sd}) is smaller than that of *syn*-CH$_3$CHOO (k_{0s}) (Table. S2 and S4) indicating a slower thermal decomposition rate of *syn*-CD$_3$CDOO, we believed that CD$_3$CDI$_2$ has been synthesized.

Details of the quantum chemistry calculation

As mentioned in the main text, we obtained the geometries for the reactants and transition states (TS) by using B3LYP/6-311+G(2d,2p), and following our previous protocol for the reactions of Criegee intermediates, we refined the energies using the QCISD(T) complete basis set (CBS) extrapolation with Dunning's basis sets, aug-cc-pVDZ, aug-cc-pVTZ and aug-cc-pVQZ.

Due to the limitation of our computational resource, we were not able to perform the aug-cc-pVQZ calculation for the syn-CH$_3$CHOO+2CH$_3$OH reaction. However, we noticed a correlation between the one methanol reaction versus the two methanol reaction for the ratio between QCISD(T)/aug-cc-pVTZ and QCISD(T)/CBS energies. We estimated the CBS value of the transition states of syn–CH$_3$CHOO+2CH$_3$OH by the following strategy: (1) we used B3LYP geometries to perform single point calculation with QCISD(T) aug-cc-pVTZ for all the transition states of CH$_2$OO+CH$_3$OH, CH$_2$OO+2CH$_3$OH, syn–CH$_3$CHOO+CH$_3$OH, and syn–CH$_3$CHOO+2CH$_3$OH. (2) For the transition states of CH$_2$OO+CH$_3$OH, CH$_2$OO+2CH$_3$OH, and syn–CH$_3$CHOO+CH$_3$OH, we performed aug-cc-pVQZ calculations and obtained the CBS energy E_{CBS}. (3) We obtained the ratio between the CBS and aug-cc-pVTZ energies, R=(E_{CBS}/E_{AVTZ}). Finally, the approximate CBS energy of the syn–CH$_3$CHOO+2CH$_3$OH system is obtained by the following equation.

$$E^{syn-CH_3CHOO}_{extrap,2CH3OH} = E^{syn-CH_3CHOO}_{AVTZ,2CH3OH} \times \frac{R^{syn-CH_3CHOO}_{1CH3OH} \times R^{CH_2OO}_{2CH3OH}}{R^{CH_2OO}_{1CH3OH}}$$

This scaling strategy is based on the assumption that the ratio of E_{CBS}/E_{AVTZ} does not depend strongly on the substituent groups of the CIs.

To test the validity of this method, we used the same method to estimate the TS energies for syn–CH$_3$CHOO+2H$_2$O and compared them with E_{CBS}, for which we still can perform the QCISD(T)/aug-cc-pVQZ calculations. The reaction barriers obtained by the above scaling method differ from the values obtained from the real CBS extrapolation only by 0.1 kcal mol^{-1}. Therefore, we think the error of the linear scaling is small compared to other uncertainties, such as the multireference effect, the partition function calculation and tunneling correction, etc.

Table S6. Zero-point corrected transition state energies (QCISD(T)/CBS//B3LYP/6-311+G(2d,2p)) for the studied reactions forming methoxymethyl hydroperoxide unless noted otherwise. The vibrational frequencies were calculated at B3LYP/6-311+G(2d,2p). The zero of the energy is set to infinitely separated reactants.

QCISD(T)/CBS in kcal mol^{-1}	a	b	c	d
anti-CH$_3$CHOO + 1CH$_3$OH	−3.85	−4.87		
syn-CH$_3$CHOO + 1CH$_3$OH	3.99	1.91	5.57*	6.10*
syn-CH$_3$CHOO + 2CH$_3$OH†	−14.45	−13.52	−11.95	−14.72
syn-CH$_3$CHOO + 2CH$_3$OD†	−14.06	−12.90	−11.28	−14.27
syn-CD$_3$CDOO + 2CH$_3$OH†	−14.72	−13.75	−12.18	−15.03

* The product is vinyl hydroperoxide.

† Approximate CBS energy. See **Details of the quantum chemistry calculation** on page S18.

Table S7. The tunneling correction factors at room temperature by using the asymmetric Eckart barrier approximations.

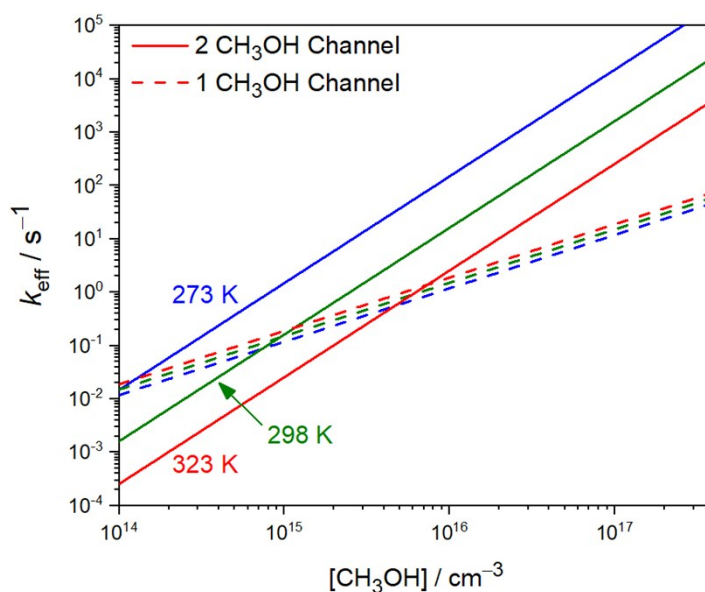| tunneling correction	2a	2b	2c	2d
syn-CH$_3$CHOO + 2CH$_3$OH	1.165	1.310	1.348	1.201
syn-CH$_3$CHOO + 2CH$_3$OD	1.145	1.243	1.262	1.172
syn-CD$_3$CDOO + 2CH$_3$OH	1.163	1.307	1.340	1.202

Fig. S12. The calculated effective decay rate coefficients of *syn*-CH$_3$CHOO reaction with 1CH$_3$OH (dashed line) and 2CH$_3$OH (solid line) at 273, 298 and 323 K.
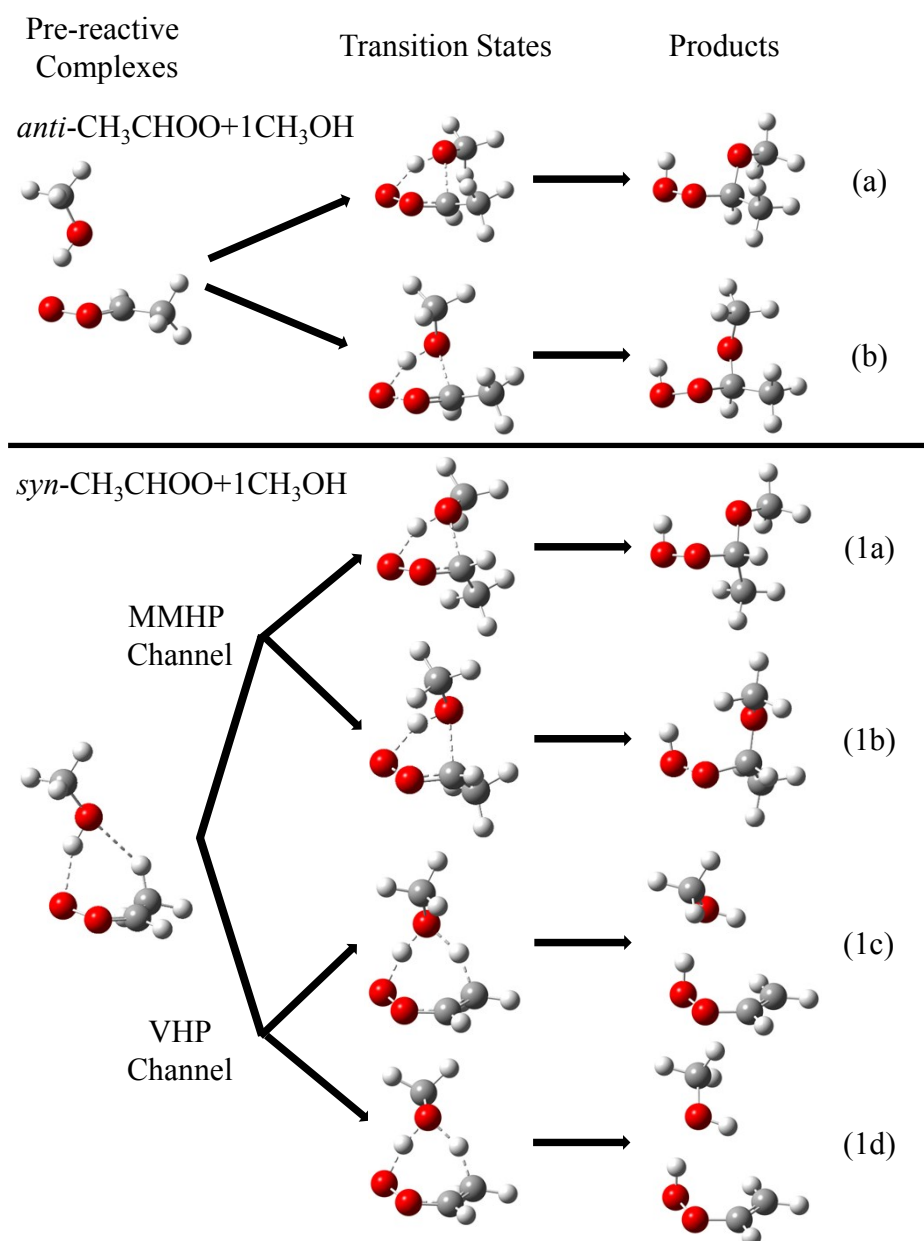
Fig. S13. Pre-reactive complex, transition state and product geometries for the reaction *anti*-CH₃CHOO+1CH₃OH and *syn*-CH₃CHOO+1CH₃OH. For *syn*-CH₃CHOO+1CH₃OH, two product channels to form either methoxymethyl hydroperoxide (MMHP) or vinyl hydroperoxide (VHP) were found. Notably, the methanol molecule acts as a catalyst for the VHP channel.

Table S8. Rotational temperatures (θ_R) and the corresponding partition functions (q_R) at 298 K for isolated CH_3OH/CH_3OD and the transition states of the reactions syn-CH_3CHOO+$2CH_3OH/CH_3OD$.

CH₃OH		CH₃OD		TS for syn-CH₃CHOO+2CH₃OH		TS for syn-CH₃CHOO+2CH₃OD	
θ_R/ K	q_R / 10^3	θ_R/ K	q_R / 10^3	θ_R/ K	q_R / 10^5	θ_R/ K	q_R / 10^5
6.1783		5.3320		0.0993		0.0985	
1.1840	3.16	1.1226	3.63	0.0732	4.57	0.0729	4.61
1.1434		1.0566		0.0549		0.0546	

Table S9. Vibrational frequencies and the corresponding partition functions at 298 K for CH_3OH/CH_3OD and the transition states (TS) of the reactions syn-CH_3CHOO+$2CH_3OH/CH_3OD$. The vibrational partition functions were calculated by using harmonic approximation. For the transition state partition functions, only the lowest 12 vibrational modes are listed since they dominate the total vibrational partition function.

CH₃OH		CH₃OD		TS for syn-CH₃CHOO+2CH₃OH		TS for syn-CH₃CHOO+2CH₃OD	
v / cm^{-1}	q_v	v / cm^{-1}	q_v	v / cm^{-1}	q_v	v / cm^{-1}	q_v
284.6	1.34	228.1	1.50	46.8	4.94	44.2	5.21
1037.9	1.01	871.3	1.02	80.1	3.12	83.4	3.02
1077.3	1.01	1041.6	1.01	95.9	2.70	95.0	2.72
1169.7	1.00	1169.6	1.00	135.6	2.08	136.3	2.07
1371.9	1.00	1247.8	1.00	142.3	2.01	142.2	2.01
1481.0	1.00	1480.8	1.00	159.4	1.86	157.7	1.88
1501.4	1.00	1501.5	1.00	174.3	1.76	181.6	1.71
1512.7	1.00	1510.9	1.00	217.5	1.54	215.4	1.55
3003.2	1.00	2804.6	1.00	224.7	1.51	223.5	1.52
3049.2	1.00	3003.9	1.00	296.0	1.32	294.6	1.32
3119.2	1.00	3049.8	1.00	328.5	1.26	323.5	1.27
3851.6	1.00	3120.3	1.00	398.5	1.17	388.5	1.18

Table S10. Calculated reaction rate coefficients as a function of temperature (in K) by using the transition state theory. The unit is $cm^6\,s^{-1}$ for termolecular reactions and $cm^3\,s^{-1}$ for bimolecular reactions. The tunneling correction has been included.

syn-CH_3CHOO + 2CH_3OH	2a	2b	2c	2d	total
223.15	2.16E-28	3.98E-29	9.42E-31	3.72E-28	6.29E-28
228.15	1.05E-28	2.00E-29	5.08E-31	1.77E-28	3.03E-28
233.15	5.28E-29	1.04E-29	2.82E-31	8.70E-29	1.50E-28
238.15	2.72E-29	5.54E-30	1.61E-31	4.42E-29	7.72E-29
243.15	1.45E-29	3.04E-30	9.44E-32	2.32E-29	4.08E-29
248.15	7.90E-30	1.71E-30	5.66E-32	1.25E-29	2.21E-29
253.15	4.42E-30	9.84E-31	3.46E-32	6.88E-30	1.23E-29
258.15	2.54E-30	5.80E-31	2.16E-32	3.90E-30	7.03E-30
263.15	1.49E-30	3.50E-31	1.38E-32	2.26E-30	4.10E-30
268.15	8.92E-31	2.16E-31	8.94E-33	1.33E-30	2.45E-30
273.15	5.46E-31	1.35E-31	5.90E-33	8.04E-31	1.49E-30
278.15	3.40E-31	8.60E-32	3.96E-33	4.94E-31	9.24E-31
283.15	2.16E-31	5.58E-32	2.70E-33	3.10E-31	5.84E-31
288.15	1.39E-31	3.68E-32	1.86E-33	1.98E-31	3.75E-31
293.15	9.08E-32	2.46E-32	1.30E-33	1.28E-31	2.45E-31
298.15	6.04E-32	1.68E-32	9.26E-34	8.42E-32	1.62E-31
303.15	4.08E-32	1.16E-32	6.66E-34	5.64E-32	1.09E-31
308.15	2.78E-32	8.08E-33	4.84E-34	3.82E-32	7.46E-32
313.15	1.93E-32	5.70E-33	3.56E-34	2.62E-32	5.16E-32
318.15	1.35E-32	4.08E-33	2.64E-34	1.82E-32	3.61E-32
323.15	9.62E-33	2.96E-33	1.99E-34	1.28E-32	2.56E-32
333.17	5.00E-33	1.60E-33	1.15E-34	6.56E-33	1.33E-32
348.09	2.04E-33	6.84E-34	5.46E-35	2.62E-33	5.40E-33
353.66	1.49E-33	5.10E-34	4.20E-35	1.90E-33	3.94E-33
360	1.06E-33	3.68E-34	3.16E-35	1.33E-33	2.79E-33

syn-CH$_3$CHOO + 2CH$_3$OD	2a	2b	2c	2d	total
223.15	5.06E-29	5.04E-30	1.01E-31	7.98E-29	1.36E-28
228.15	2.50E-29	2.62E-30	5.62E-32	3.88E-29	6.65E-29
233.15	1.28E-29	1.39E-30	3.24E-32	1.95E-29	3.37E-29
238.15	6.70E-30	7.64E-31	1.91E-32	1.01E-29	1.76E-29
243.15	3.62E-30	4.30E-31	1.15E-32	5.40E-30	9.45E-30
248.15	2.00E-30	2.50E-31	7.10E-33	2.96E-30	5.21E-30
253.15	1.14E-30	1.47E-31	4.48E-33	1.66E-30	2.95E-30
258.15	6.62E-31	8.88E-32	2.86E-33	9.52E-31	1.71E-30
263.15	3.92E-31	5.48E-32	1.88E-33	5.60E-31	1.01E-30
268.15	2.38E-31	3.44E-32	1.25E-33	3.36E-31	6.11E-31
273.15	1.47E-31	2.20E-32	8.44E-34	2.06E-31	3.76E-31
278.15	9.28E-32	1.44E-32	5.78E-34	1.29E-31	2.36E-31
283.15	5.96E-32	9.52E-33	4.04E-34	8.16E-32	1.51E-31
288.15	3.88E-32	6.40E-33	2.86E-34	5.28E-32	9.82E-32
293.15	2.56E-32	4.36E-33	2.04E-34	3.46E-32	6.49E-32
298.15	1.73E-32	3.02E-33	1.48E-34	2.30E-32	4.35E-32
303.15	1.18E-32	2.12E-33	1.08E-34	1.56E-32	2.96E-32
308.15	8.12E-33	1.50E-33	8.02E-35	1.07E-32	2.04E-32
313.15	5.68E-33	1.08E-33	6.00E-35	7.44E-33	1.43E-32
318.15	4.02E-33	7.86E-34	4.54E-35	5.22E-33	1.01E-32
323.15	2.88E-33	5.76E-34	3.48E-35	3.72E-33	7.22E-33
333.17	1.53E-33	3.20E-34	2.08E-35	1.94E-33	3.81E-33
348.09	6.40E-34	1.43E-34	1.03E-35	7.98E-34	1.59E-33
353.66	4.72E-34	1.08E-34	8.08E-36	5.84E-34	1.17E-33
360	3.38E-34	7.96E-35	6.18E-36	4.16E-34	8.39E-34

syn-CD₃CDOO + 2CH₃OH	2a	2b	2c	2d	total
223.15	3.26E-28	5.18E-29	1.19E-30	6.44E-28	1.02E-27
228.15	1.56E-28	2.58E-29	6.34E-31	3.02E-28	4.85E-28
233.15	7.74E-29	1.32E-29	3.50E-31	1.47E-28	2.38E-28
238.15	3.94E-29	6.96E-30	1.97E-31	7.36E-29	1.20E-28
243.15	2.08E-29	3.78E-30	1.14E-31	3.80E-29	6.26E-29
248.15	1.12E-29	2.10E-30	6.78E-32	2.02E-29	3.35E-29
253.15	6.20E-30	1.20E-30	4.12E-32	1.10E-29	1.84E-29
258.15	3.52E-30	7.02E-31	2.54E-32	6.14E-30	1.04E-29
263.15	2.04E-30	4.20E-31	1.61E-32	3.52E-30	5.99E-30
268.15	1.21E-30	2.56E-31	1.03E-32	2.06E-30	3.53E-30
273.15	7.34E-31	1.59E-31	6.76E-33	1.23E-30	2.13E-30
278.15	4.52E-31	1.01E-31	4.50E-33	7.48E-31	1.31E-30
283.15	2.84E-31	6.48E-32	3.04E-33	4.64E-31	8.16E-31
288.15	1.82E-31	4.24E-32	2.10E-33	2.92E-31	5.19E-31
293.15	1.18E-31	2.82E-32	1.46E-33	1.88E-31	3.36E-31
298.15	7.80E-32	1.90E-32	1.03E-33	1.23E-31	2.21E-31
303.15	5.22E-32	1.30E-32	7.34E-34	8.12E-32	1.47E-31
308.15	3.54E-32	9.04E-33	5.30E-34	5.46E-32	9.96E-32
313.15	2.44E-32	6.36E-33	3.88E-34	3.72E-32	6.83E-32
318.15	1.70E-32	4.52E-33	2.86E-34	2.56E-32	4.74E-32
323.15	1.20E-32	3.26E-33	2.14E-34	1.79E-32	3.34E-32
333.17	6.16E-33	1.74E-33	1.23E-34	9.04E-33	1.71E-32
348.09	2.46E-33	7.34E-34	5.72E-35	3.54E-33	6.79E-33
353.66	1.79E-33	5.42E-34	4.38E-35	2.54E-33	4.92E-33
360	1.26E-33	3.90E-34	3.28E-35	1.77E-33	3.46E-33

syn-CH$_3$CHOO + CH$_3$OH	1a	1b	1c	1d	total
273.15	1.30E-18	5.97E-17	6.83E-18	2.78E-18	7.07E-17
278.15	1.48E-18	6.35E-17	6.69E-18	2.74E-18	7.44E-17
283.15	1.67E-18	6.74E-17	6.62E-18	2.71E-18	7.85E-17
288.15	1.89E-18	7.15E-17	6.60E-18	2.72E-18	8.27E-17
293.15	2.12E-18	7.57E-17	6.62E-18	2.74E-18	8.72E-17
298.15	2.37E-18	8.00E-17	6.68E-18	2.78E-18	9.18E-17
303.15	2.65E-18	8.45E-17	6.78E-18	2.83E-18	9.68E-17
308.15	2.94E-18	8.91E-17	6.92E-18	2.90E-18	1.02E-16
313.15	3.27E-18	9.38E-17	7.10E-18	2.99E-18	1.07E-16
318.15	3.62E-18	9.87E-17	7.31E-18	3.09E-18	1.13E-16
323.15	3.99E-18	1.04E-16	7.54E-18	3.21E-18	1.18E-16
328.15	4.39E-18	1.09E-16	7.81E-18	3.35E-18	1.24E-16
333.15	4.82E-18	1.14E-16	8.11E-18	3.50E-18	1.31E-16
338.15	5.28E-18	1.20E-16	8.44E-18	3.66E-18	1.37E-16
343.15	5.78E-18	1.25E-16	8.81E-18	3.84E-18	1.44E-16
348.15	6.30E-18	1.31E-16	9.20E-18	4.04E-18	1.51E-16
353.15	6.86E-18	1.37E-16	9.63E-18	4.25E-18	1.58E-16
358.15	7.46E-18	1.43E-16	1.01E-17	4.48E-18	1.65E-16
363.15	8.09E-18	1.49E-16	1.06E-17	4.73E-18	1.73E-16
368.15	8.76E-18	1.55E-16	1.11E-17	5.00E-18	1.80E-16
373.15	9.47E-18	1.62E-16	1.17E-17	5.29E-18	1.88E-16
378.15	1.02E-17	1.69E-16	1.23E-17	5.59E-18	1.97E-16

anti-CH$_3$CHOO + CH$_3$OH	a	b	total
273.15	4.57E-12	1.98E-11	2.43E-11
278.15	4.01E-12	1.67E-11	2.07E-11
283.15	3.54E-12	1.43E-11	1.78E-11
288.15	3.14E-12	1.22E-11	1.54E-11
293.15	2.79E-12	1.05E-11	1.33E-11
298.15	2.50E-12	9.14E-12	1.16E-11
303.15	2.24E-12	7.96E-12	1.02E-11
308.15	2.02E-12	6.97E-12	8.99E-12
313.15	1.83E-12	6.13E-12	7.96E-12
318.15	1.66E-12	5.42E-12	7.08E-12
323.15	1.52E-12	4.81E-12	6.33E-12
328.15	1.39E-12	4.29E-12	5.67E-12
333.15	1.27E-12	3.84E-12	5.11E-12
338.15	1.17E-12	3.45E-12	4.62E-12
343.15	1.08E-12	3.10E-12	4.18E-12
348.15	9.99E-13	2.81E-12	3.81E-12
353.15	9.27E-13	2.55E-12	3.47E-12
358.15	8.62E-13	2.32E-12	3.18E-12
363.15	8.03E-13	2.11E-12	2.92E-12
368.15	7.50E-13	1.94E-12	2.69E-12
373.15	7.03E-13	1.78E-12	2.48E-12
378.15	6.59E-13	1.63E-12	2.29E-12

Representative time traces for the reaction of *syn*-CH₃CHOO with CH₃OH vapor
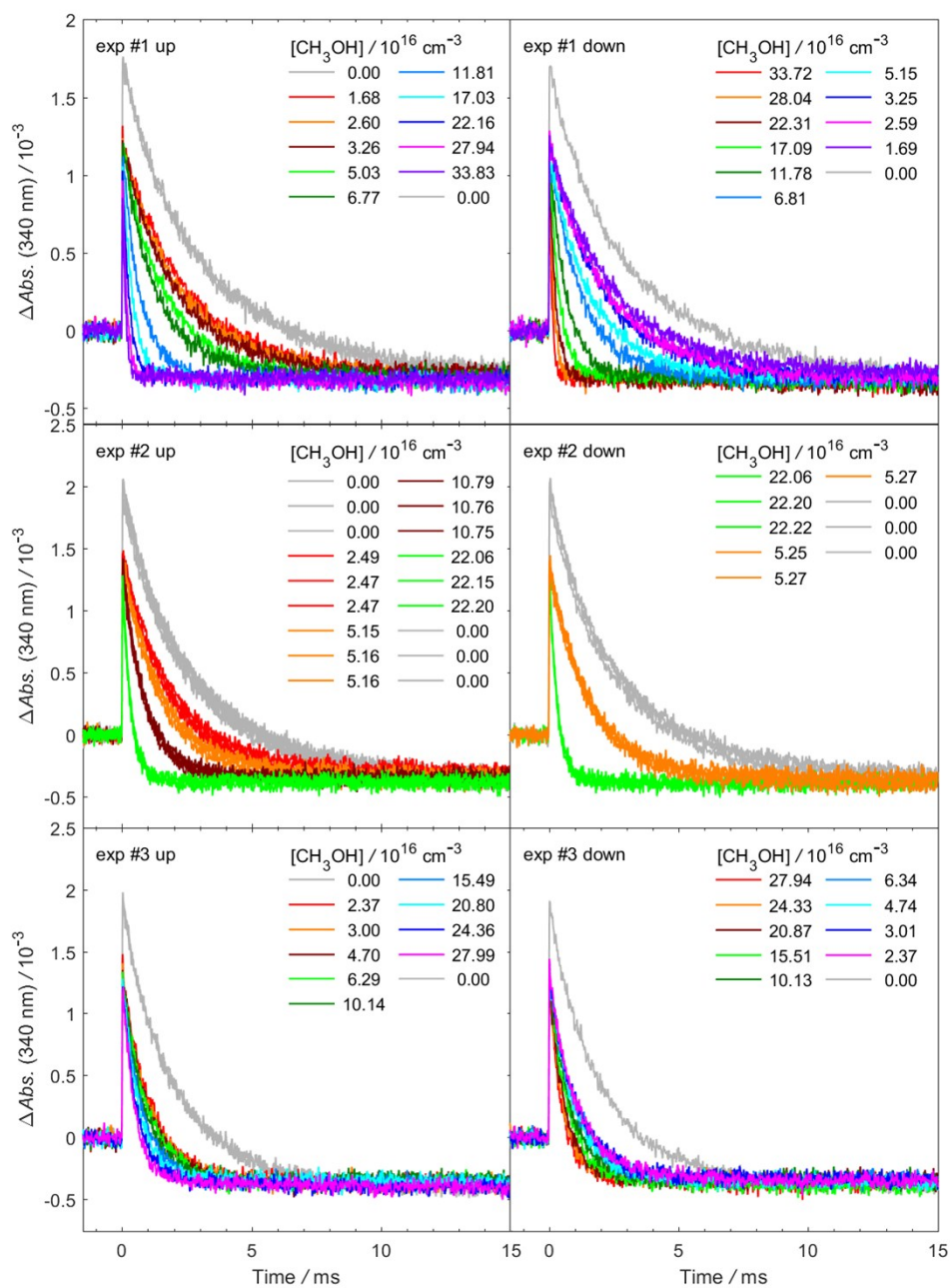
Fig. S14. Representative time traces of CH_3CHOO at 340 ± 5 nm under different $[CH_3OH]$ (exp# 1-3). The photolysis laser pulse sets the time zero. In each experiment, $[CH_3OH]$ was scanned from 0 to the maximum (labeled as "up") and from the maximum to 0 (labeled as "down"). $[CH_3CHOO]_0$ was determined by the traces when $[CH_3OH] = 0$ cm⁻³ (gray lines). At high $[CH_3OH]$, only the signal of *syn*-CH_3CHOO was observed. The negative baseline was caused by the depletion of the precursor CH_3CHI_2.
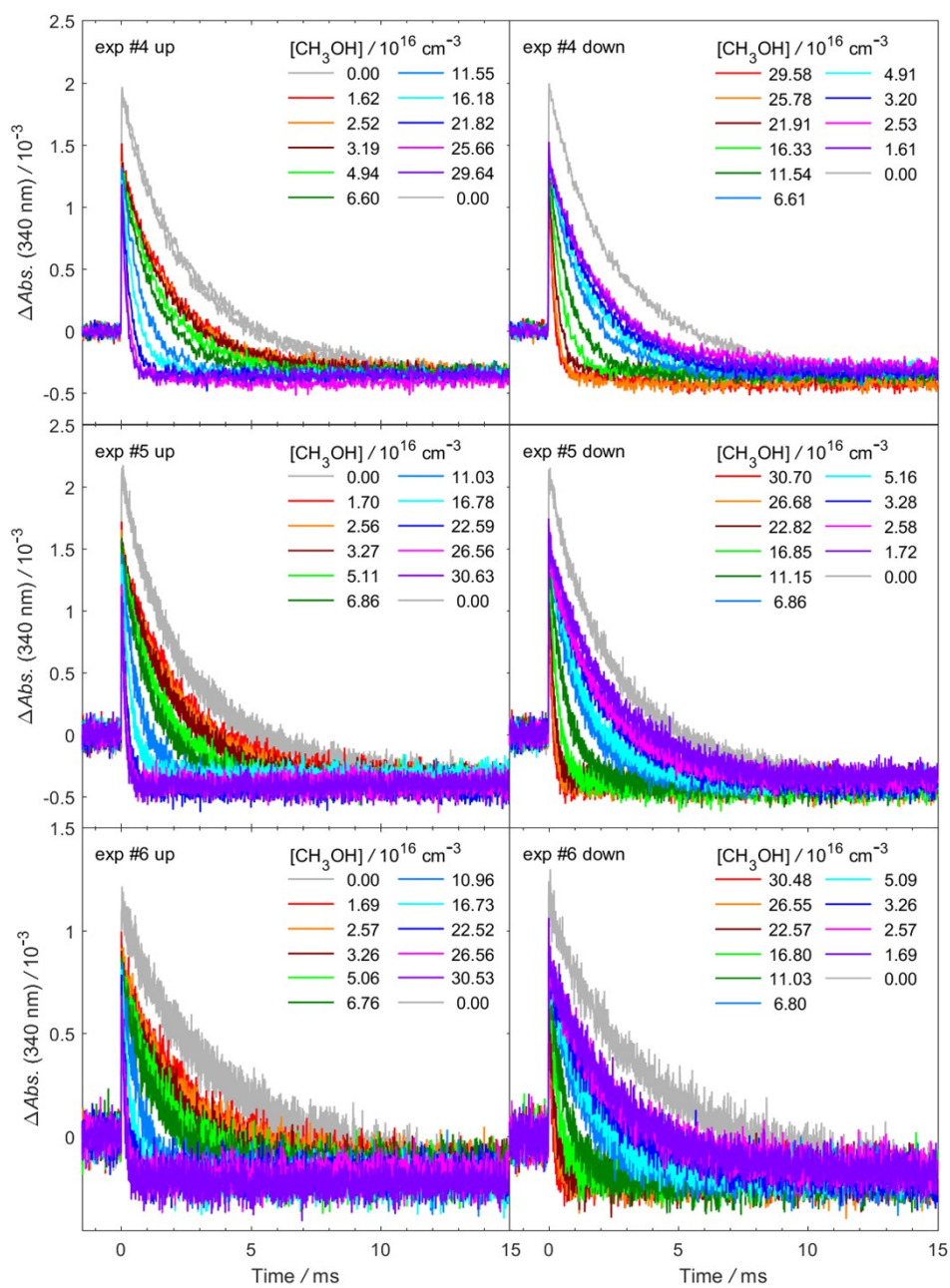
Fig. S15. As Fig. S14, but different experiment sets (exp# 4-6).
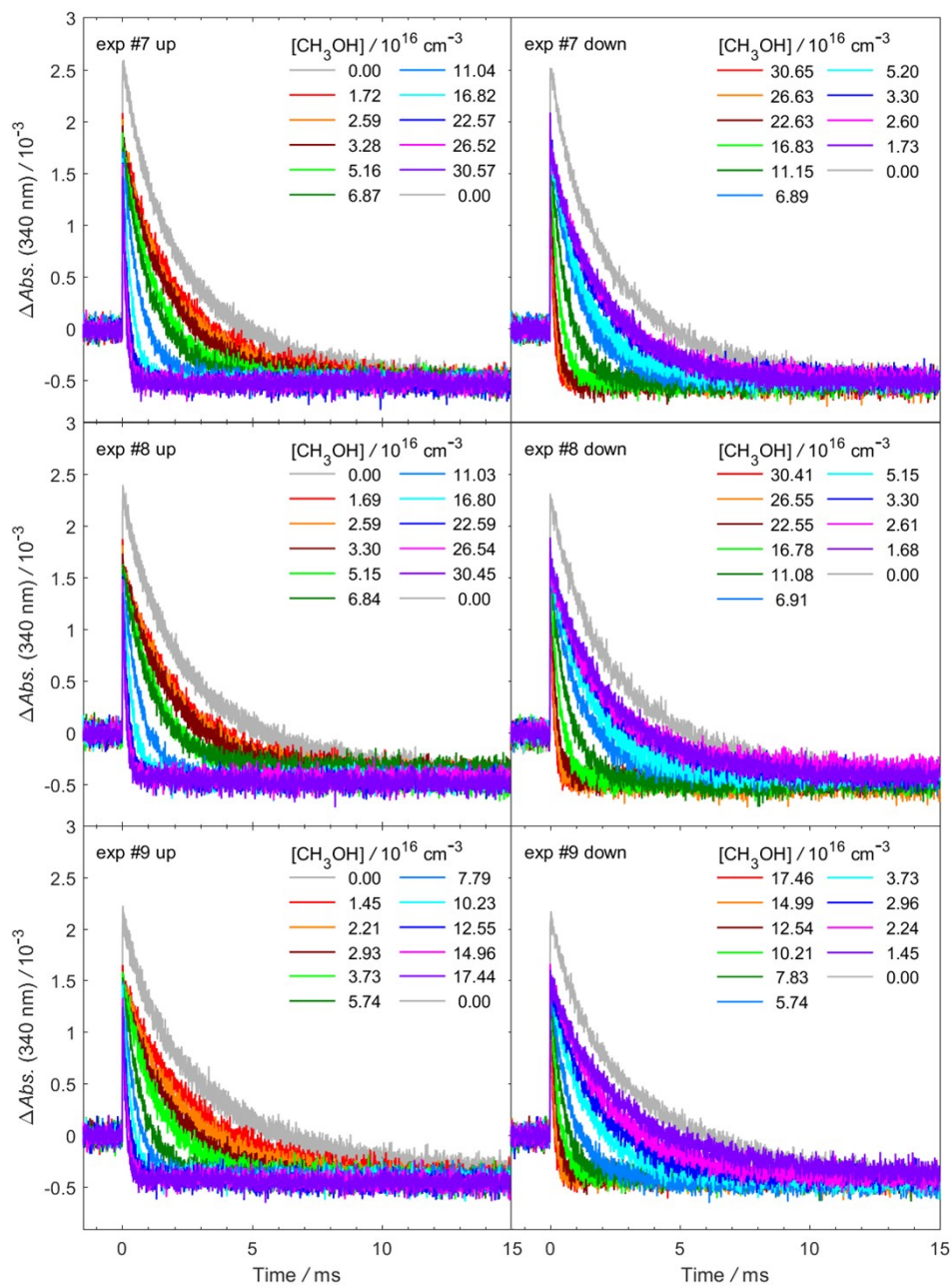
Fig. S16. As Fig. S14, but different experiment sets (exp# 7-9).
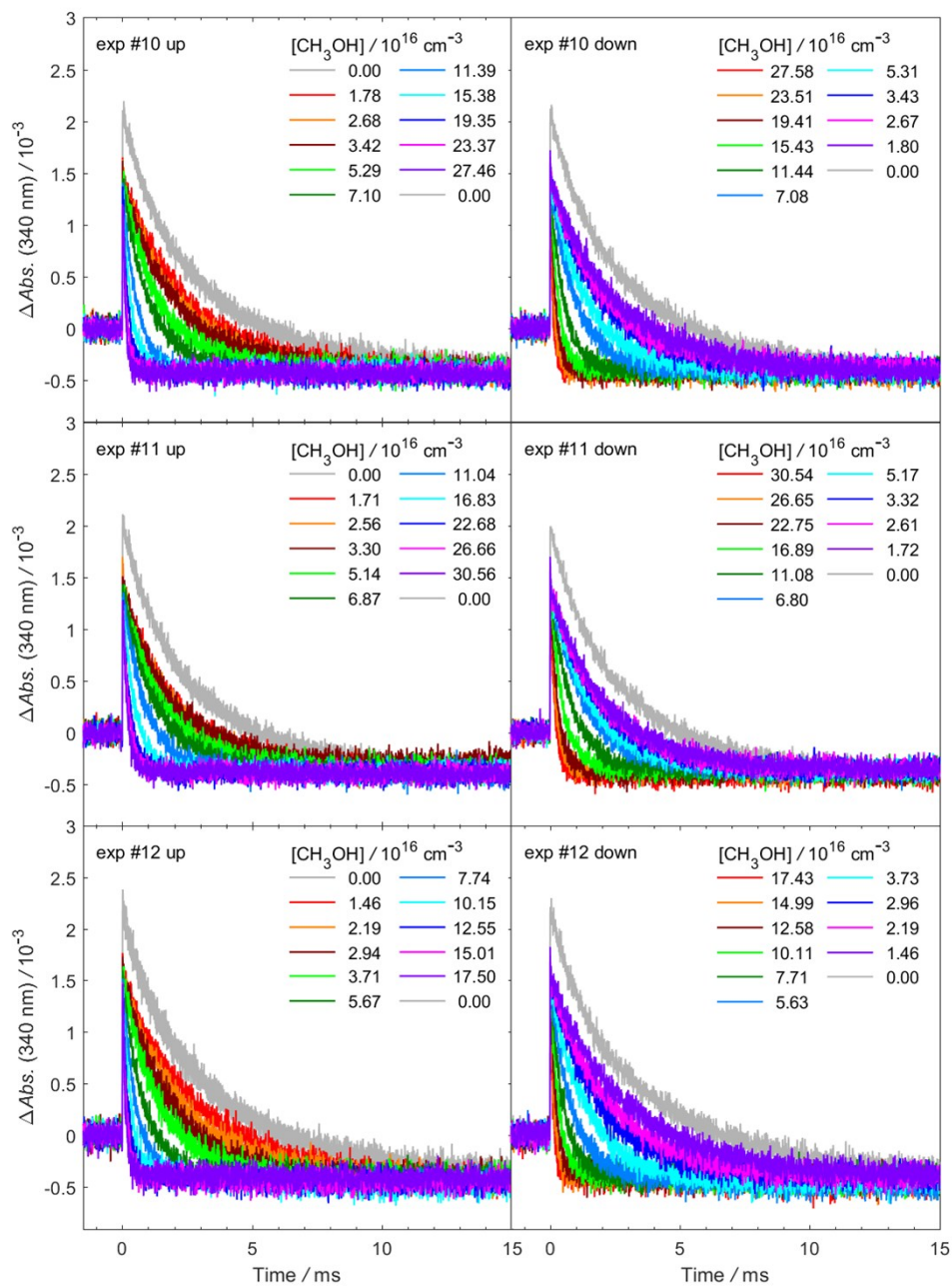
Fig. S17. As Fig. S14, but different experiment sets (exp# 10-12).
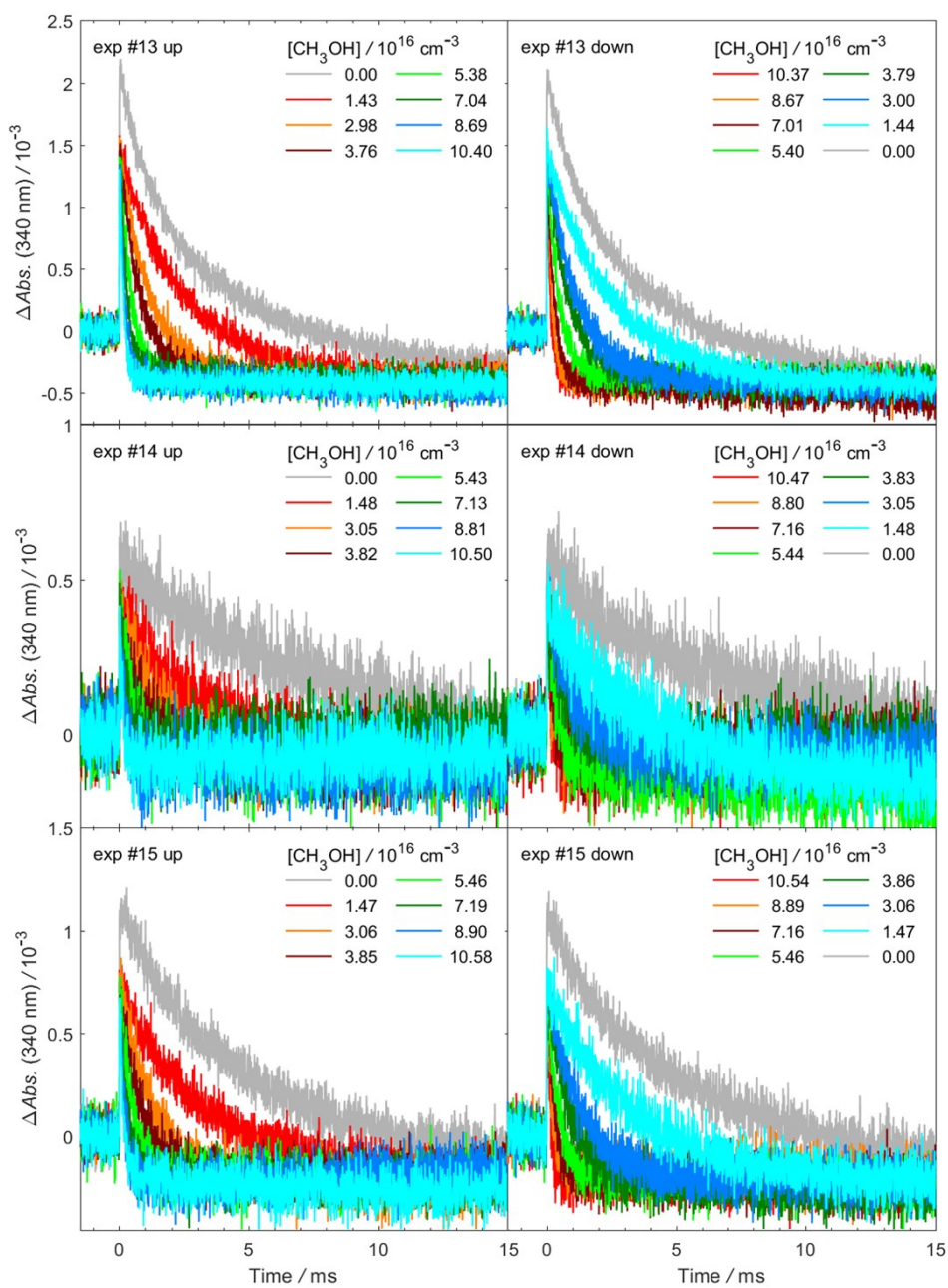
Fig. S18. As Fig. S14, but different experiment sets (exp# 13-15).
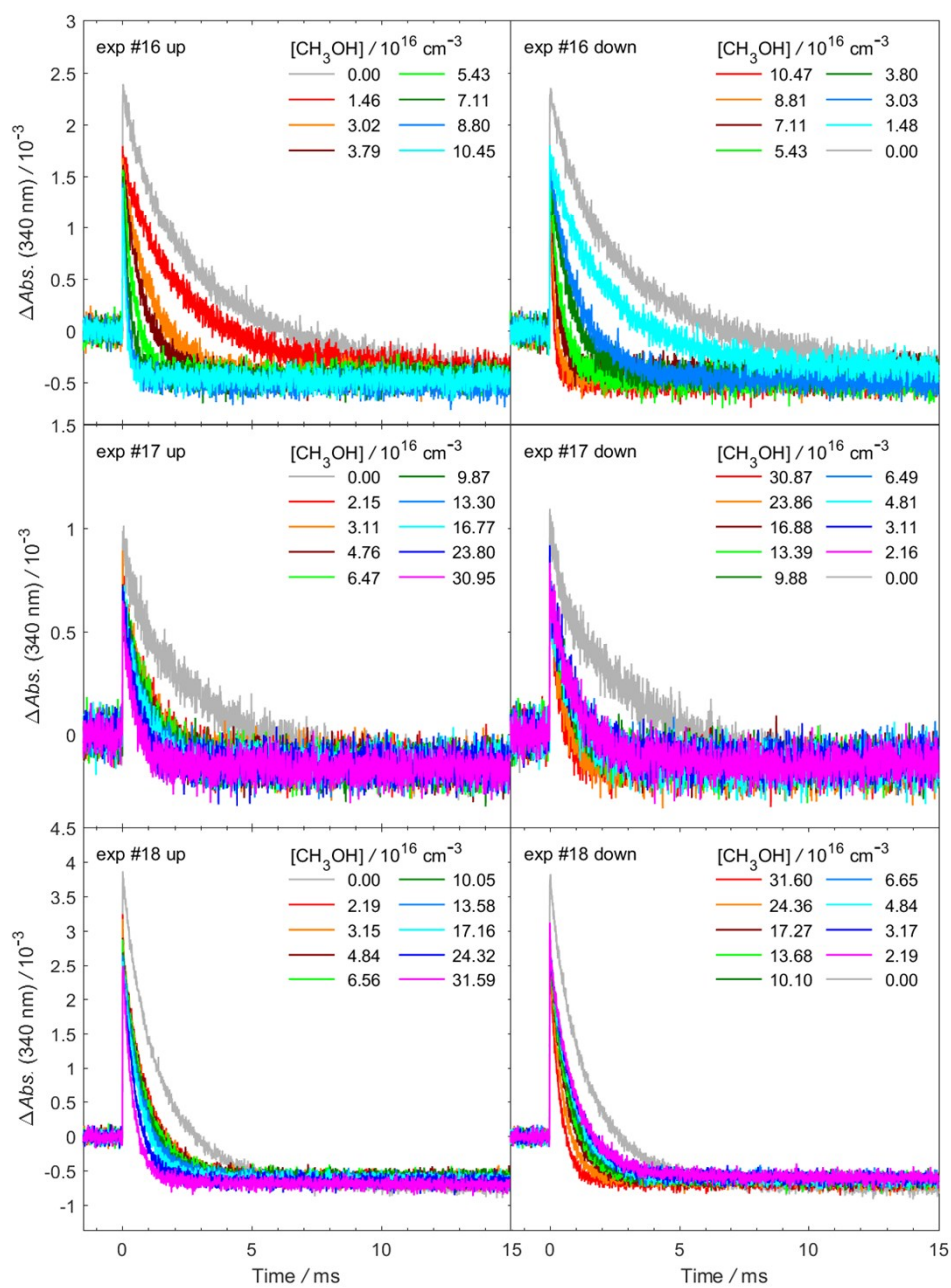
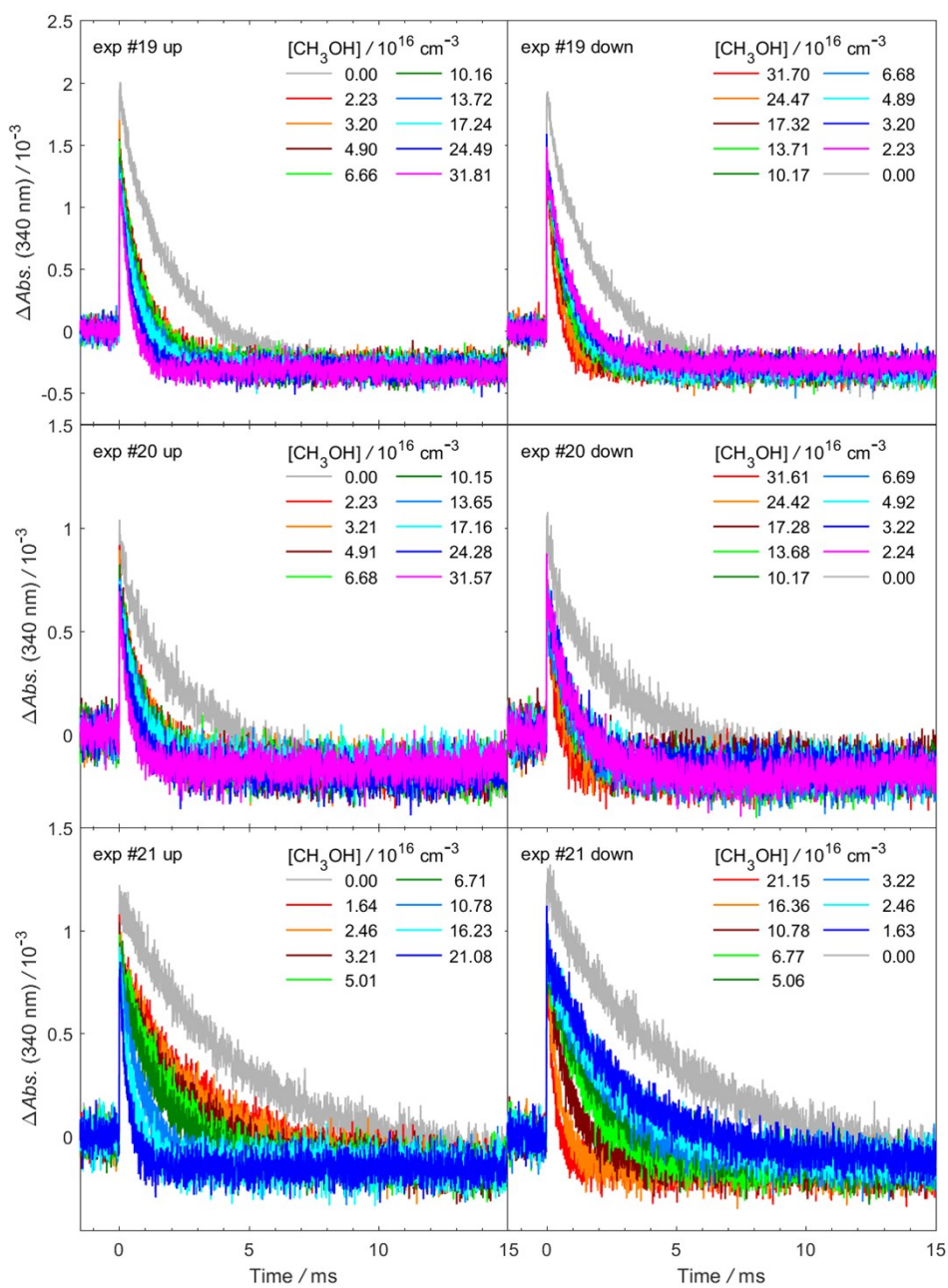**Fig. S19.** As Fig. S14, but different experiment sets (exp# 16-18).

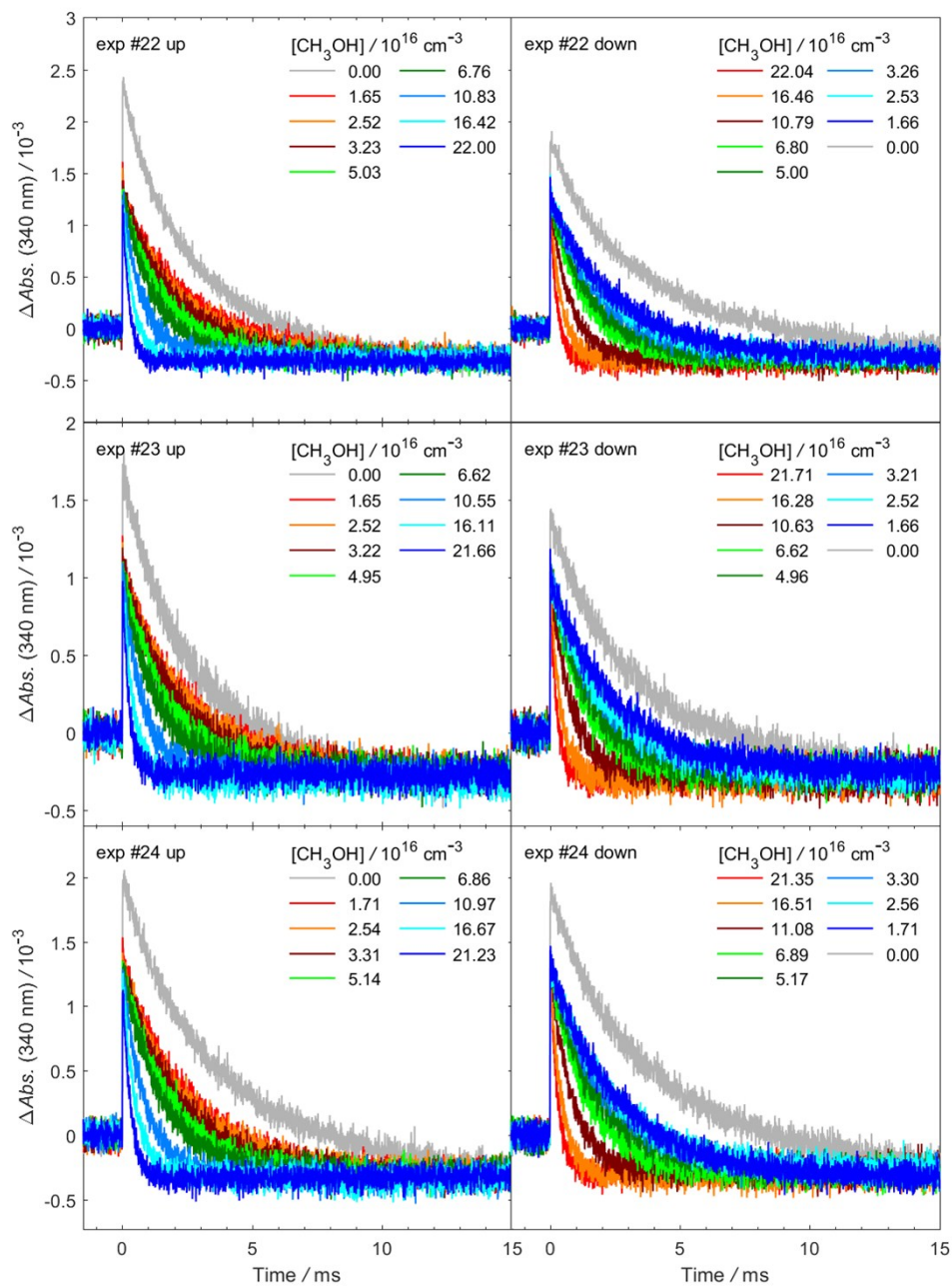**Fig. S20.** As Fig. S14, but different experiment sets (exp# 19-21).

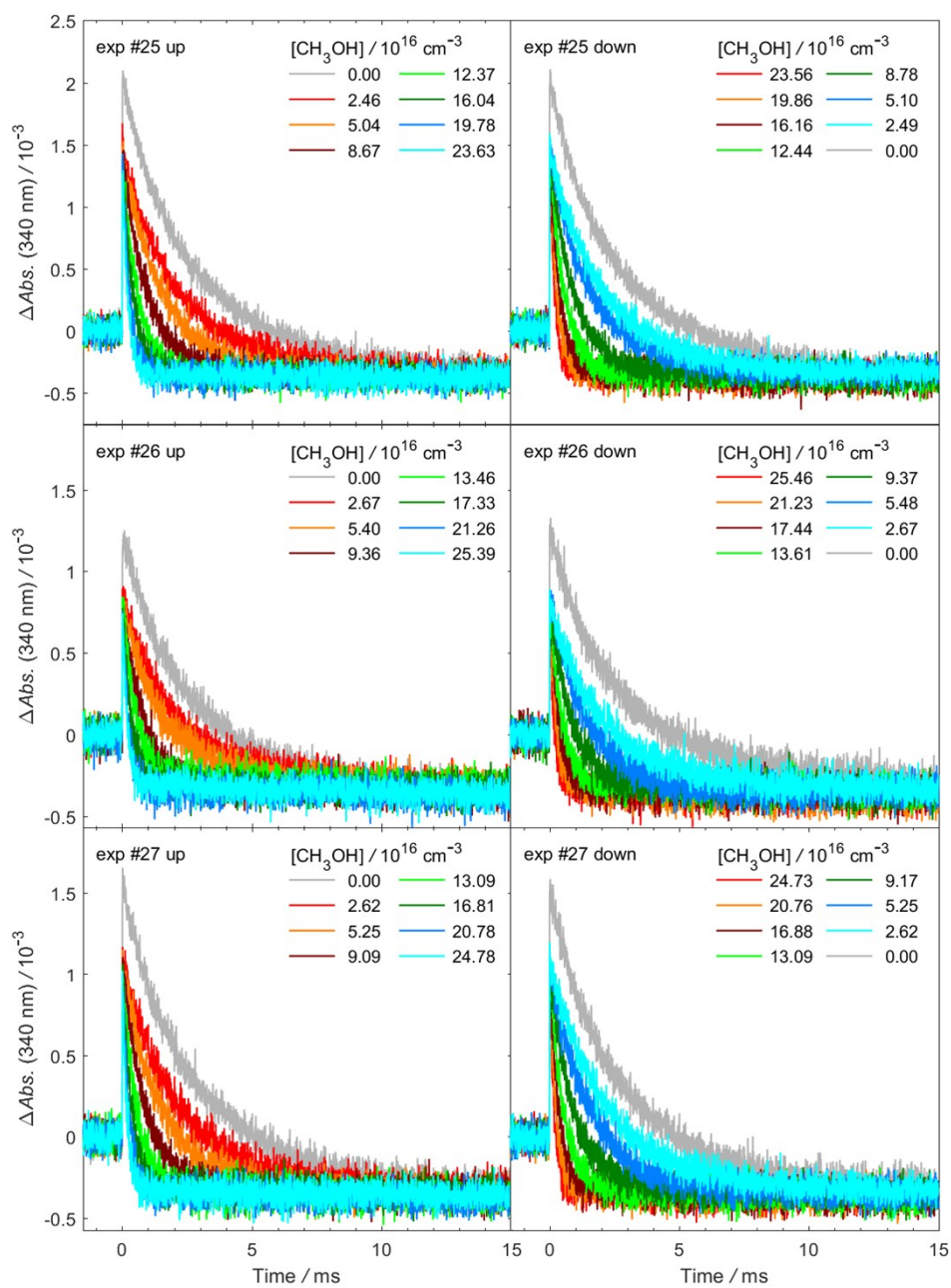**Fig. S21.** As Fig. S14, but different experiment sets (exp# 22-24).

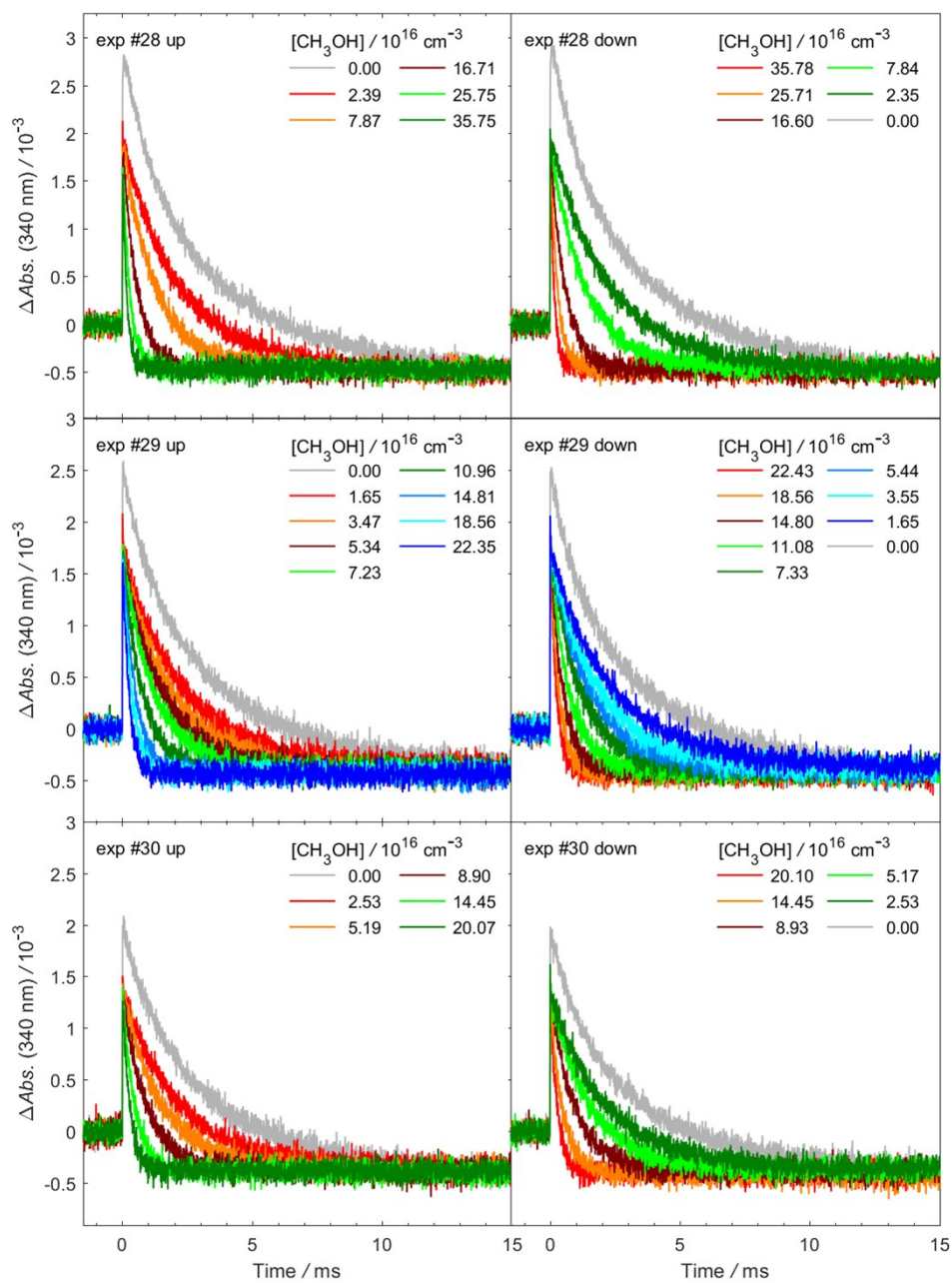**Fig. S22.** As Fig. S14, but different experiment sets (exp# 25-27).

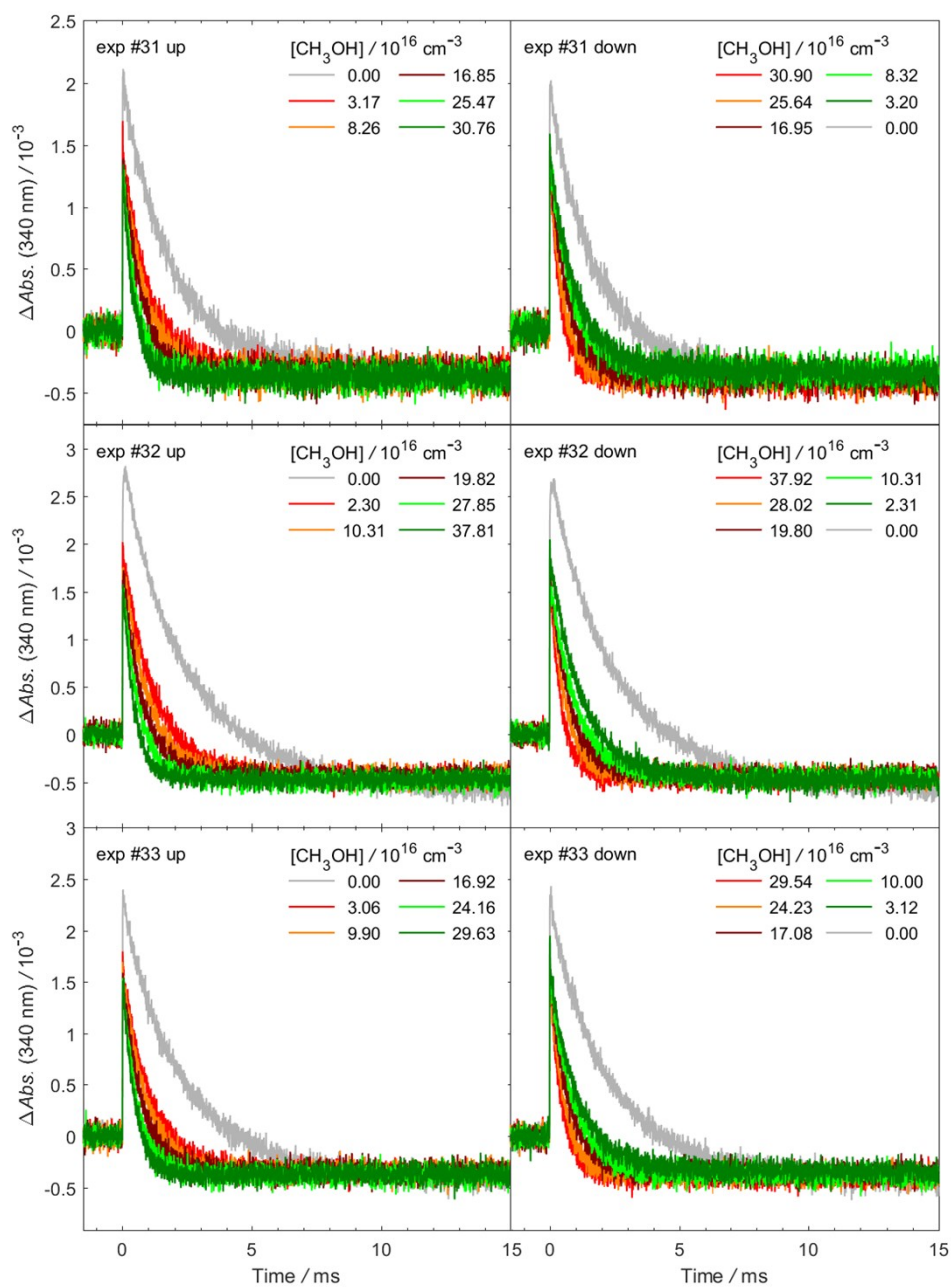**Fig. S23.** As Fig. S14, but different experiment sets (exp# 28-30).

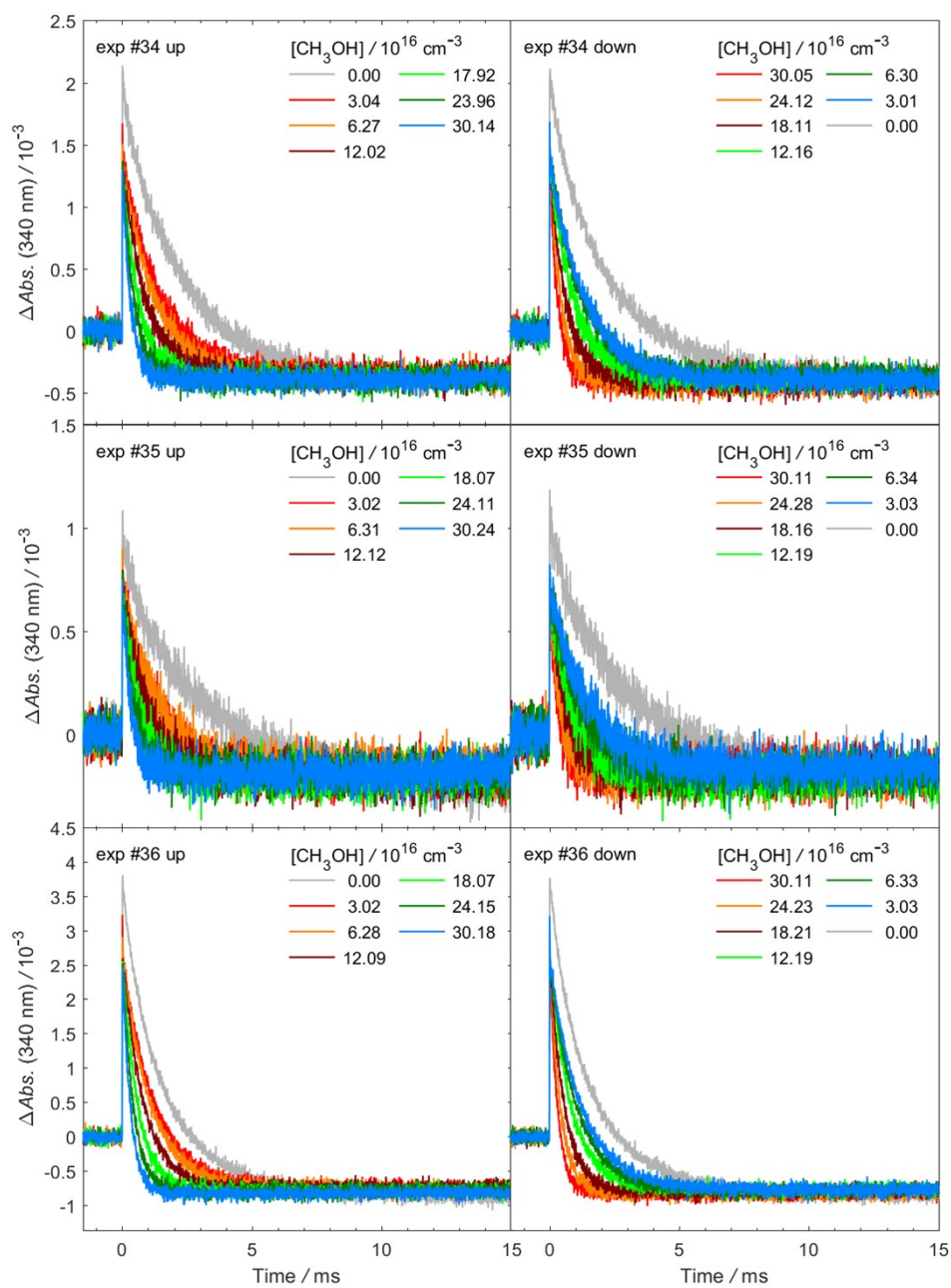**Fig. S24.** As Fig. S14, but different experiment sets (exp# 31-33).

Fig. S25. As Fig. S14, but different experiment sets (exp# 34-36).

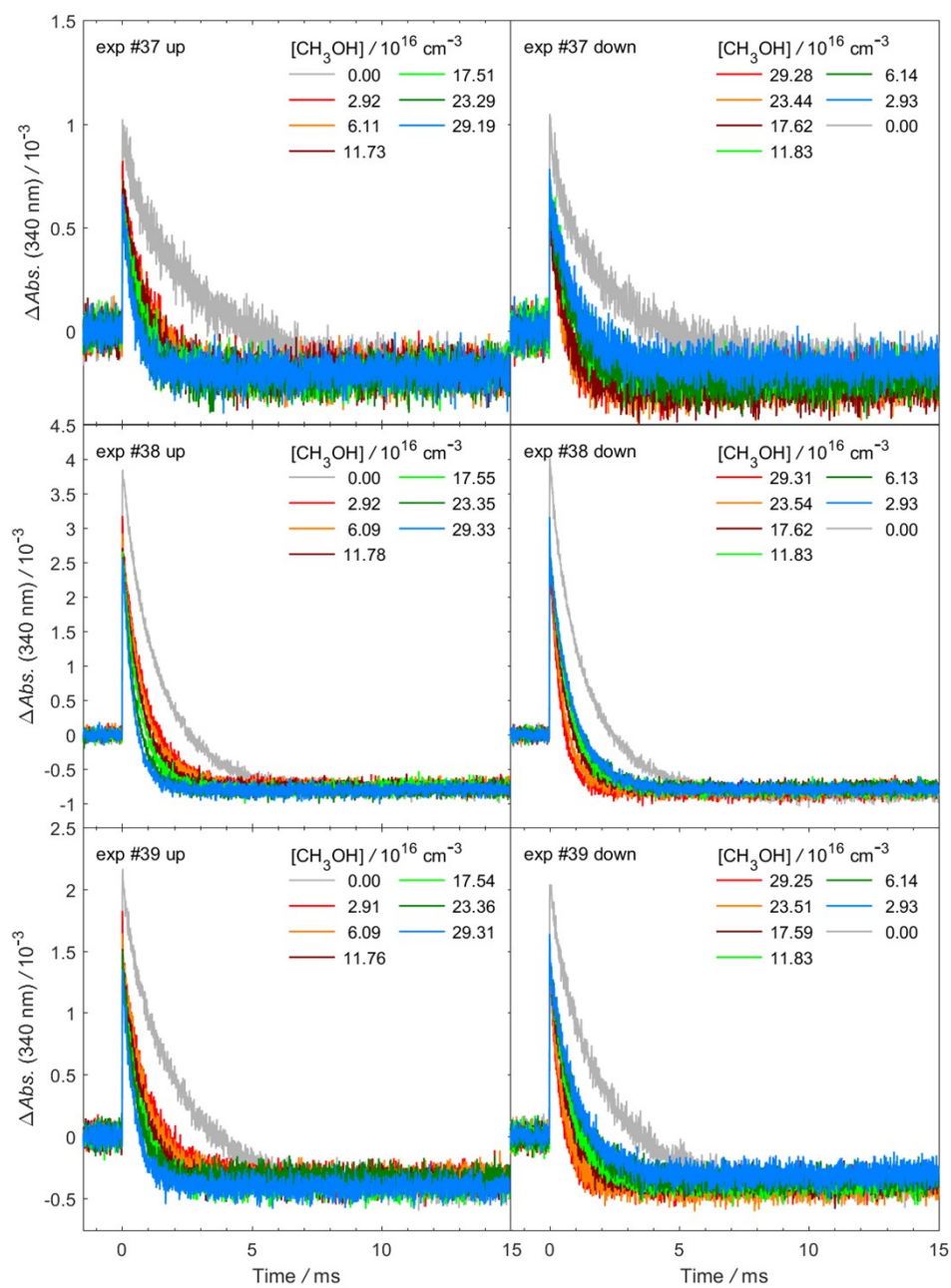**Fig. S26.** As Fig. S14, but different experiment sets (exp# 37-39).

Representative time traces for the reaction of *syn*-CH₃CHOO with CH₃OD vapor
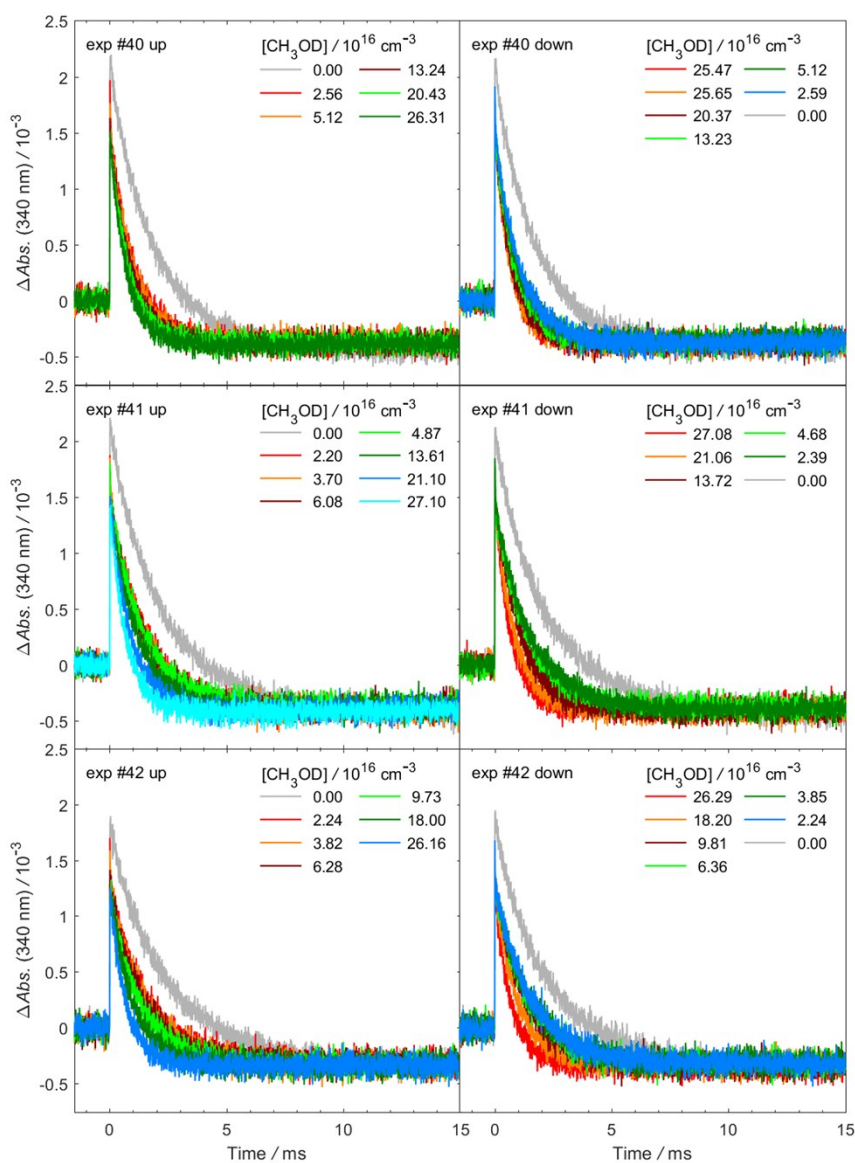

Fig. S27. Representative time traces of CH_3CHOO at 340 ± 5 nm under different $[CH_3OD]$ (exp# 40-42). The photolysis laser pulse sets the time zero. In each experiment, $[CH_3OD]$ was scanned from 0 to the maximum (labeled as "up") and from the maximum to 0 (labeled as "down"). $[CH_3CHOO]_0$ was determined by the traces when $[CH_3OD] = 0$ cm^{-3} (gray lines). At high $[CH_3OD]$, only the signal of *syn*-CH_3CHOO was observed. The negative baseline was caused by the depletion of the precursor CH_3CHI_2.
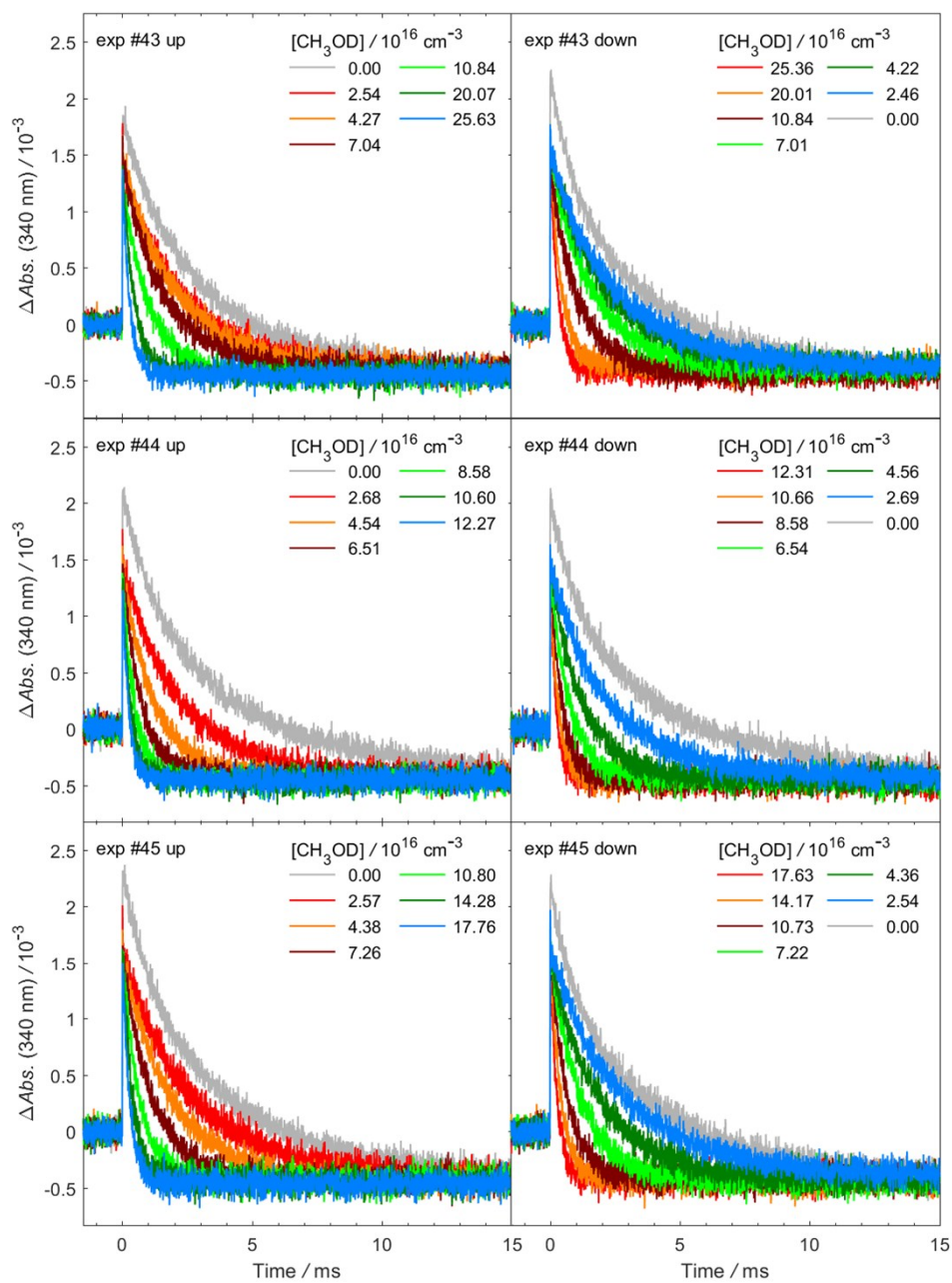
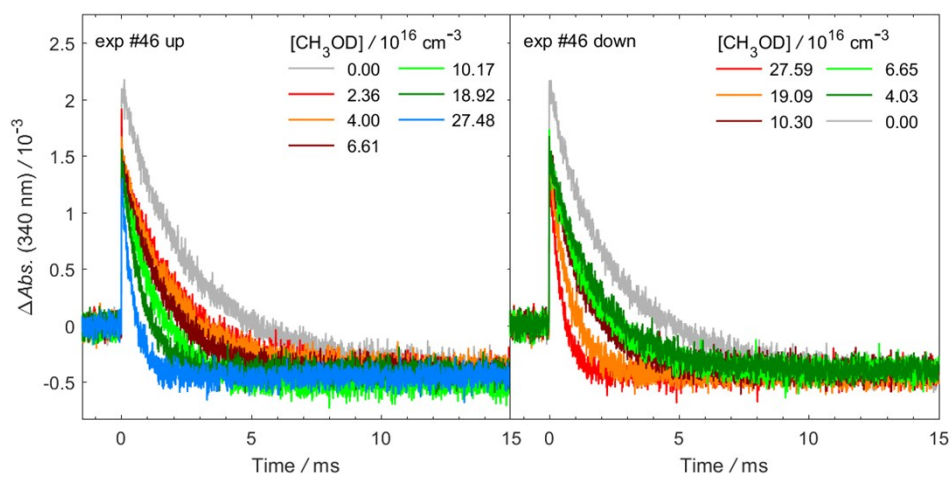**Fig. S28.** As Fig. S27 but different experiment sets (exp# 43-45)..

Fig. S29. As Fig. S27 but different experiment sets (exp# 46).

Representative time traces for the reaction of *syn*-CD₃CDOO with CH₃OH vapor

Fig. S30. Representative time traces of CD_3CDOO at 340 ± 5 nm under different $[CH_3OH]$ (exp# 47-48). The photolysis laser pulse sets the time zero. In each experiment, $[CH_3OH]$ was scanned from 0 to the maximum (labeled as "up") and from the maximum to 0 (labeled as "down"). $[CD_3CDOO]_0$ was determined by the traces when $[CH_3OH] = 0$ cm^{-3} (gray lines). At high $[CH_3OH]$, only the signal of *syn*-CD_3CDOO was observed. The negative baseline was caused by the depletion of the precursor CD_3CDI_2.

Representative time traces for the reaction of *anti*-CH₃CHOO with CH₃OH
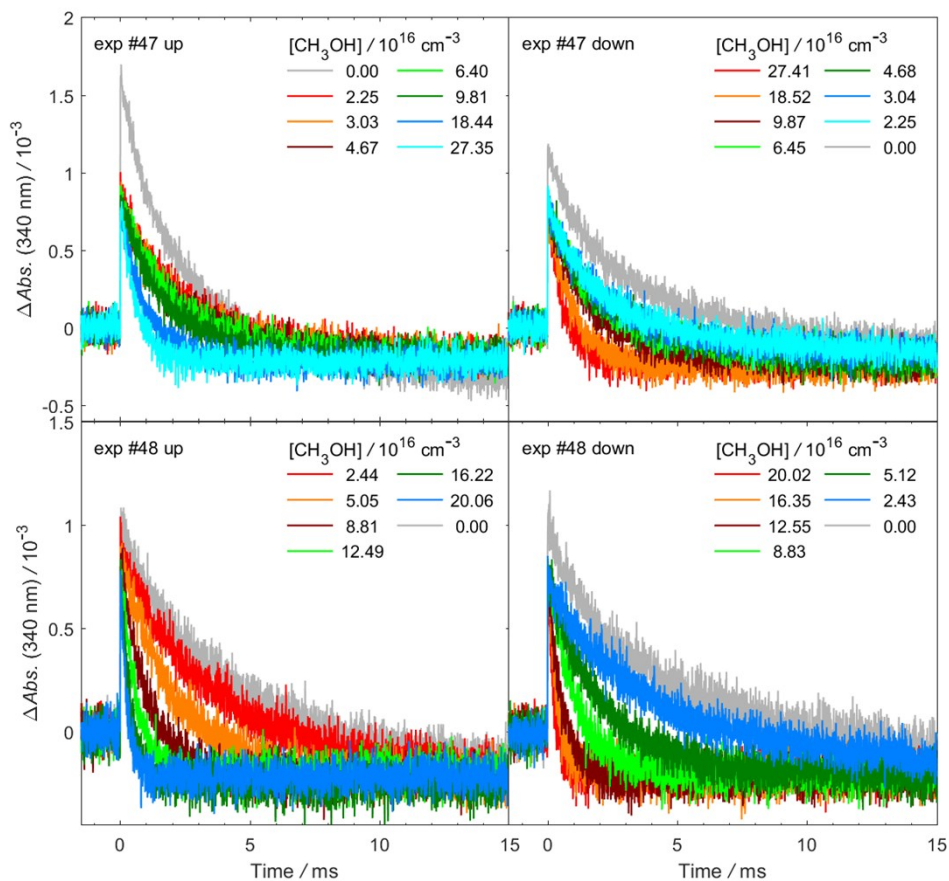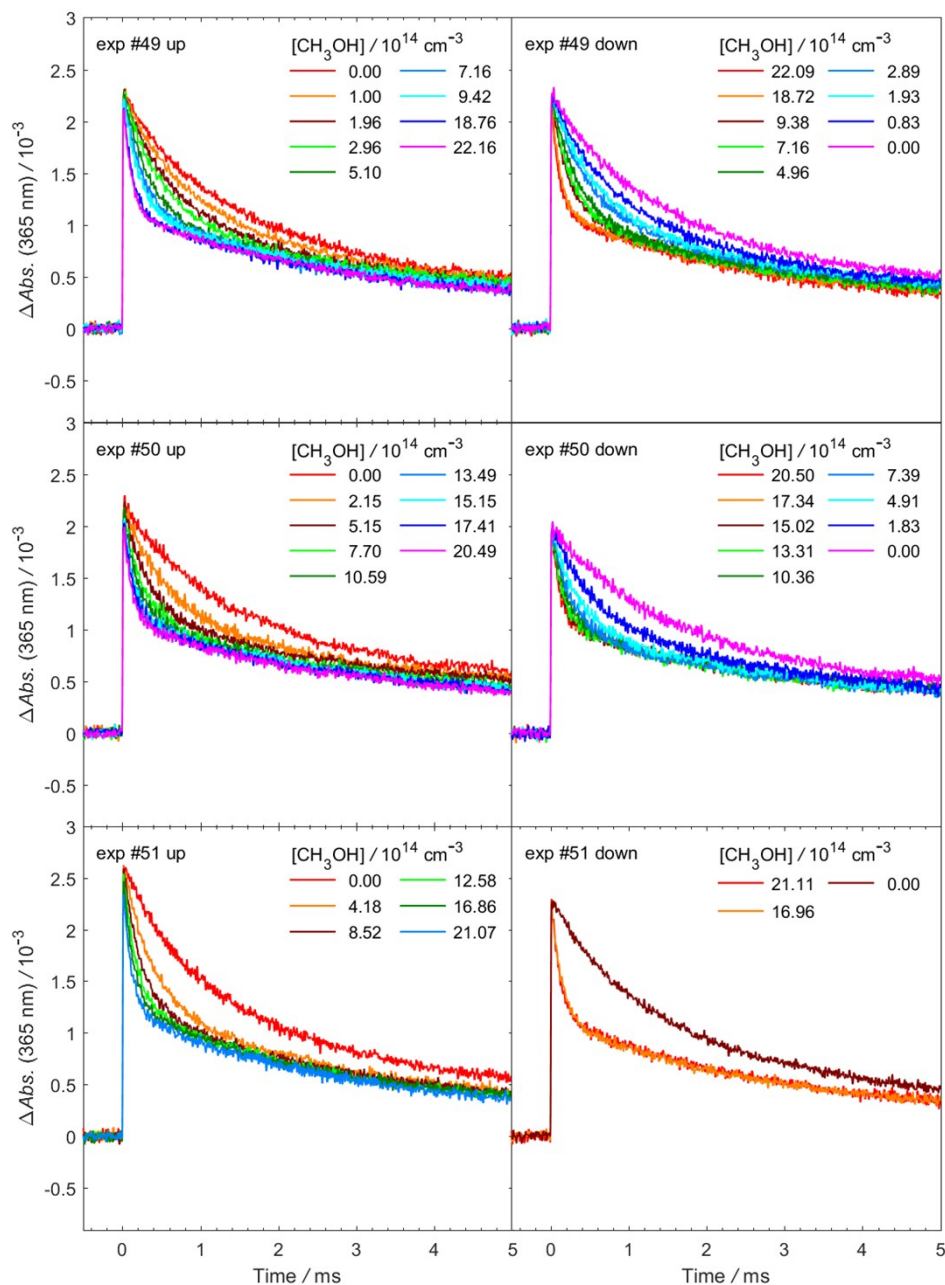

Fig. S31. Representative time traces of CH₃CHOO at 365±5 nm under different [CH₃OH] (exp# 49-51). The photolysis laser pulse sets the time zero. In each experiment, [CH₃OH] was scanned from 0 to the maximum (labeled as "up") and from the maximum to 0 (labeled as "down"). At low [CH₃OH], the consumption of *syn*-CH₃CHOO by CH₃OH is negligible.
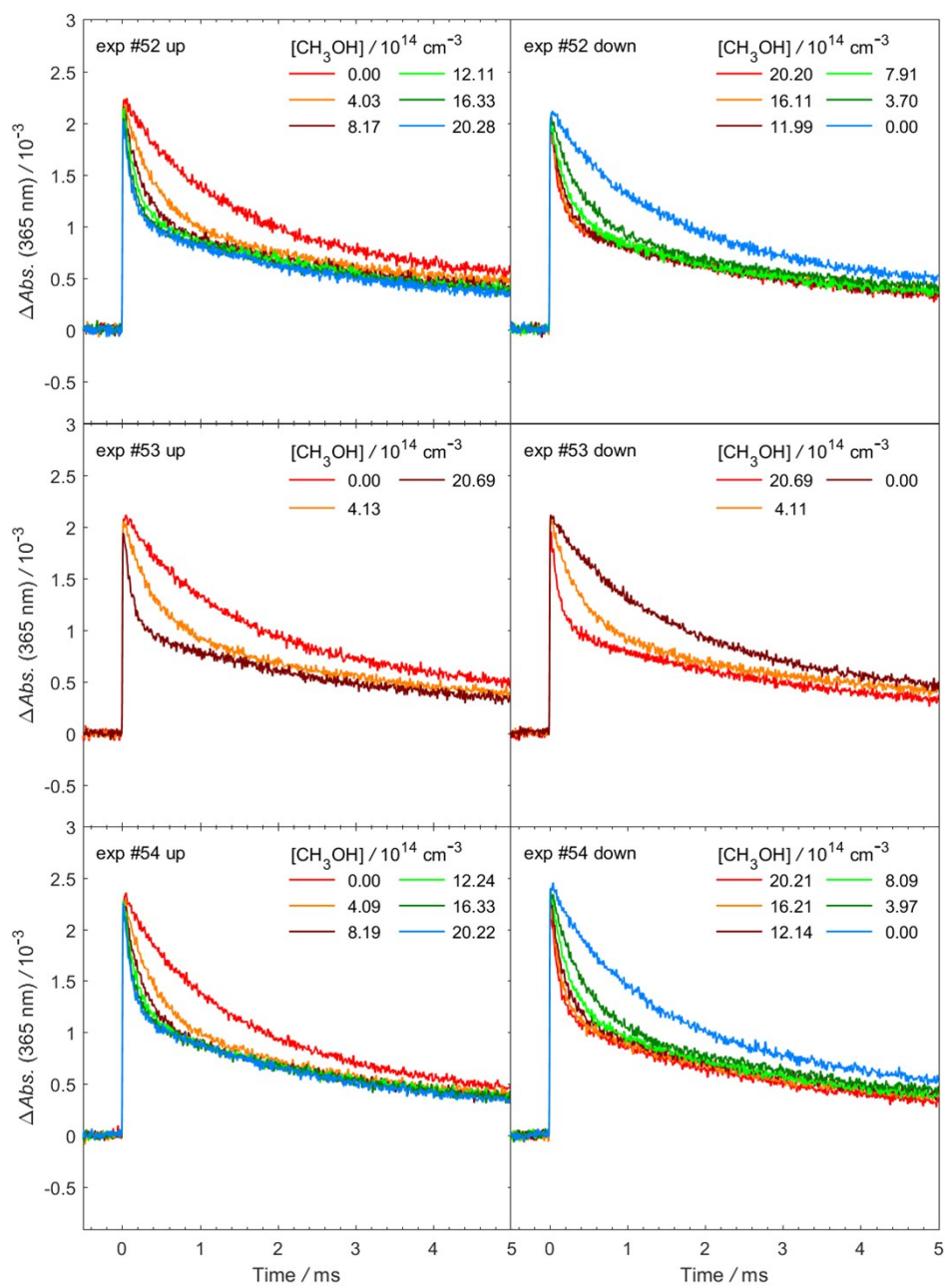
Fig. S32. As Fig. S31 but different experiment sets (exp# 52-54).
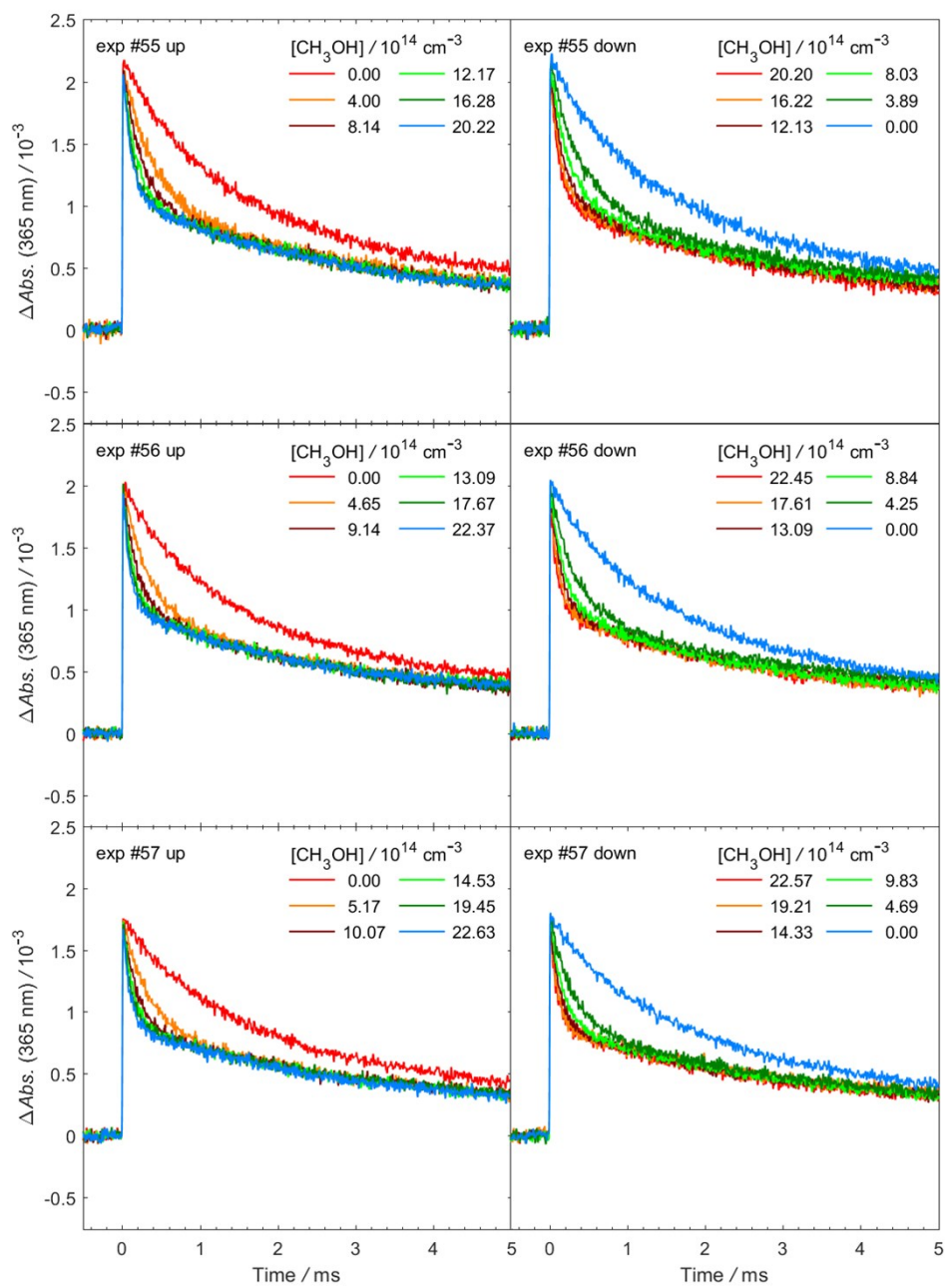
Fig. S33. As Fig. S31 but different experiment sets (exp# 55-57).

Fig. S34. As Fig. S31 but different experiment sets (exp# 58-60).
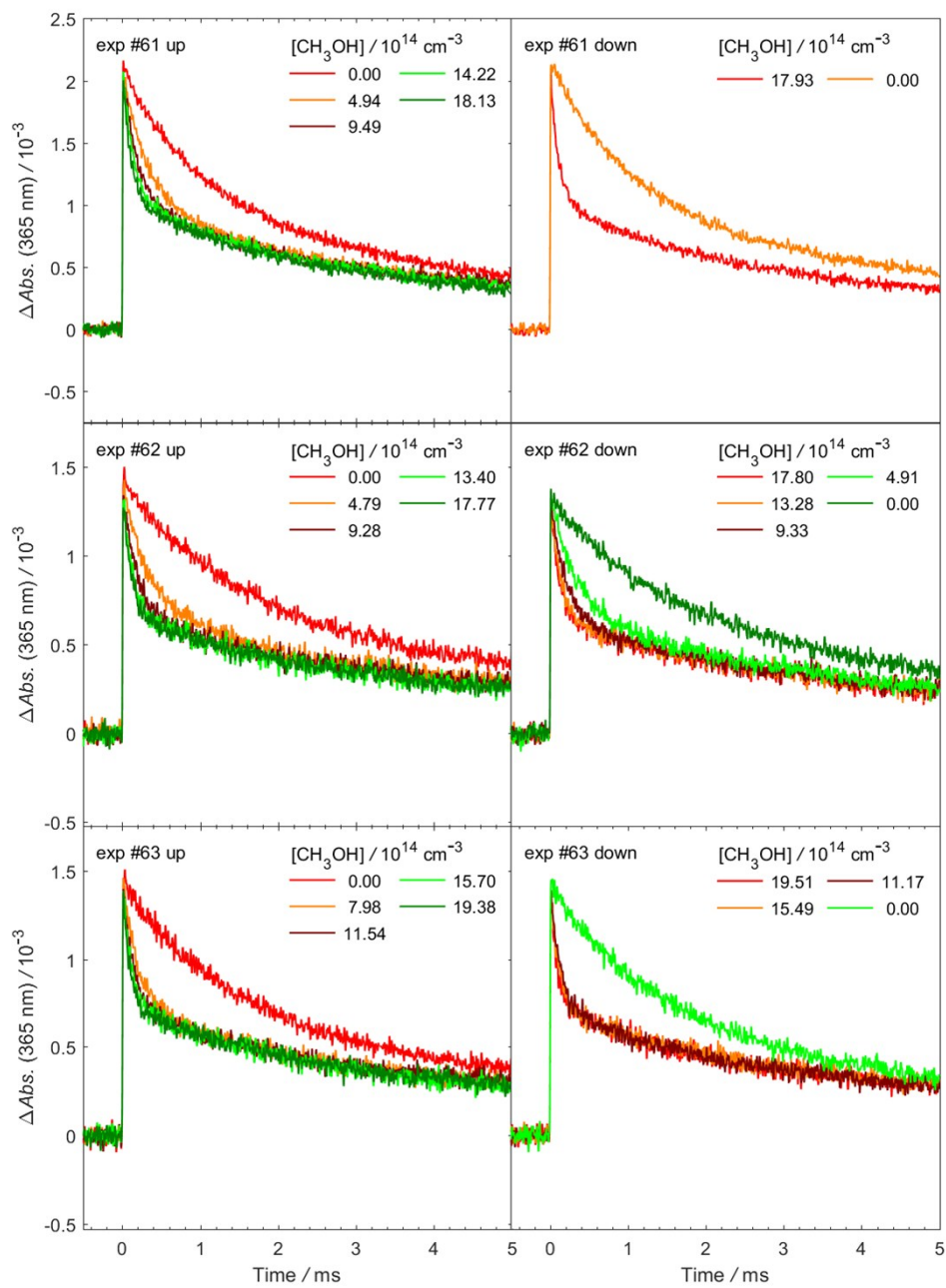
Fig. S35. As Fig. S31 but different experiment sets (exp# 61-63).
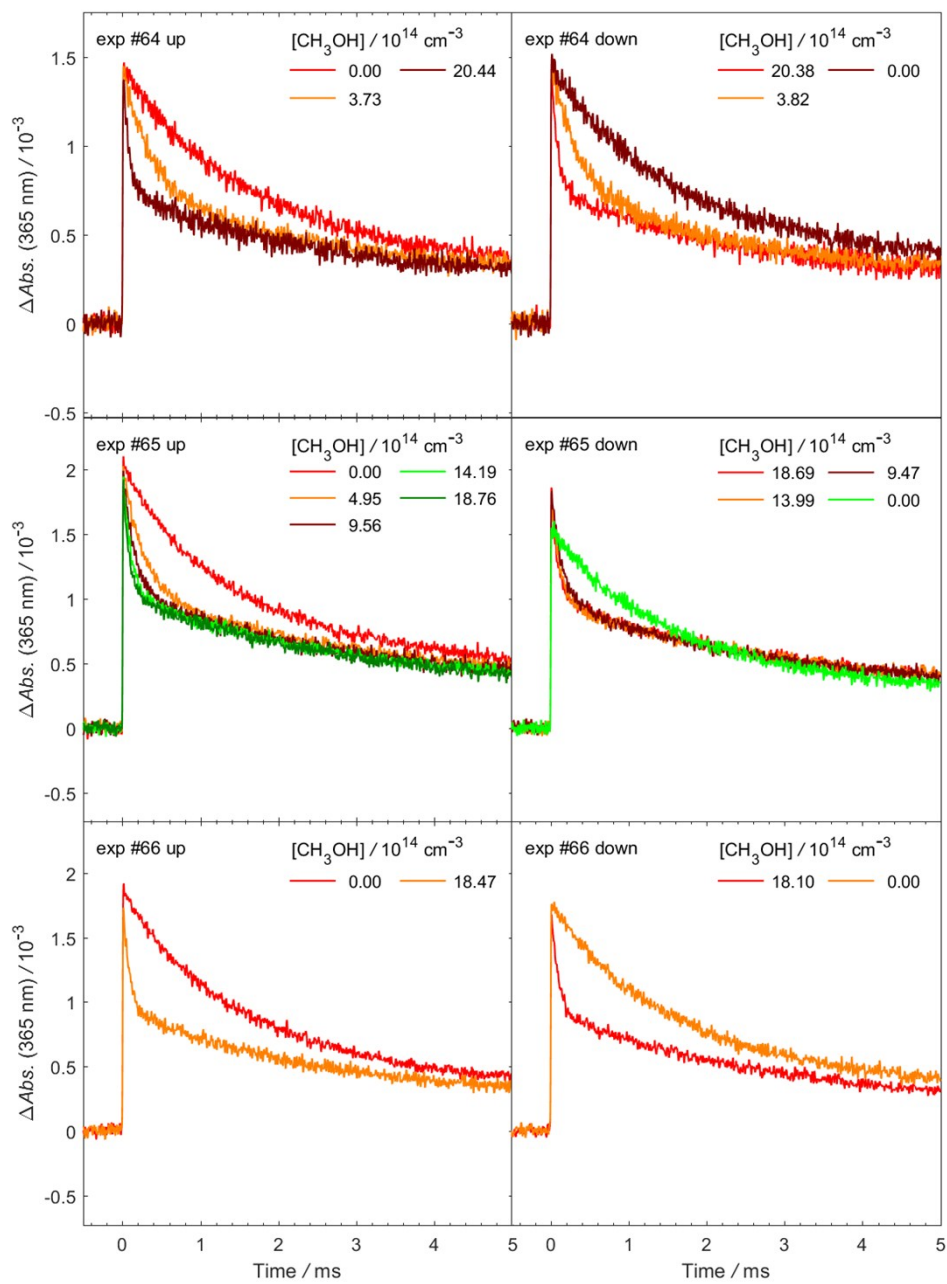
Fig. S36. As Fig. S31 but different experiment sets (exp# 64-66).
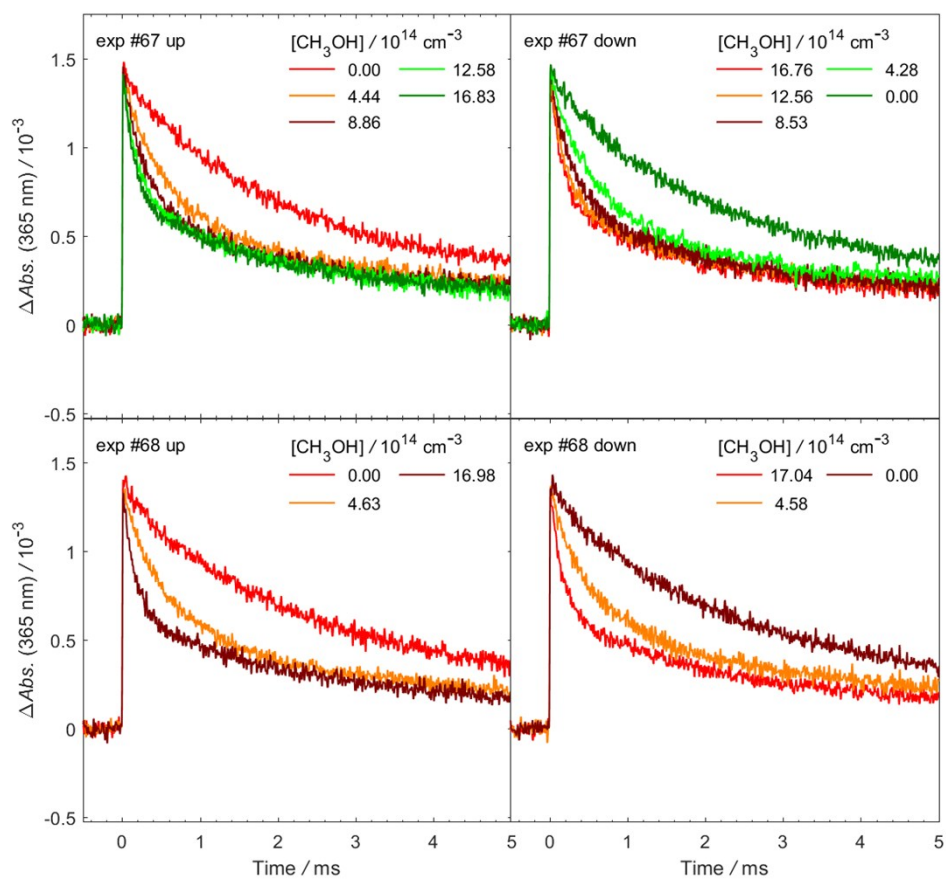
Fig. S37. As Fig. S31 but different experiment sets (exp# 67-68).

Table S11. XYZ geometries (in Ångström) for the reactants (*syn*-CH₃CHOO, CH₃OH) and the transition states, optimized at B3LYP/6-311+G(2d,2p).

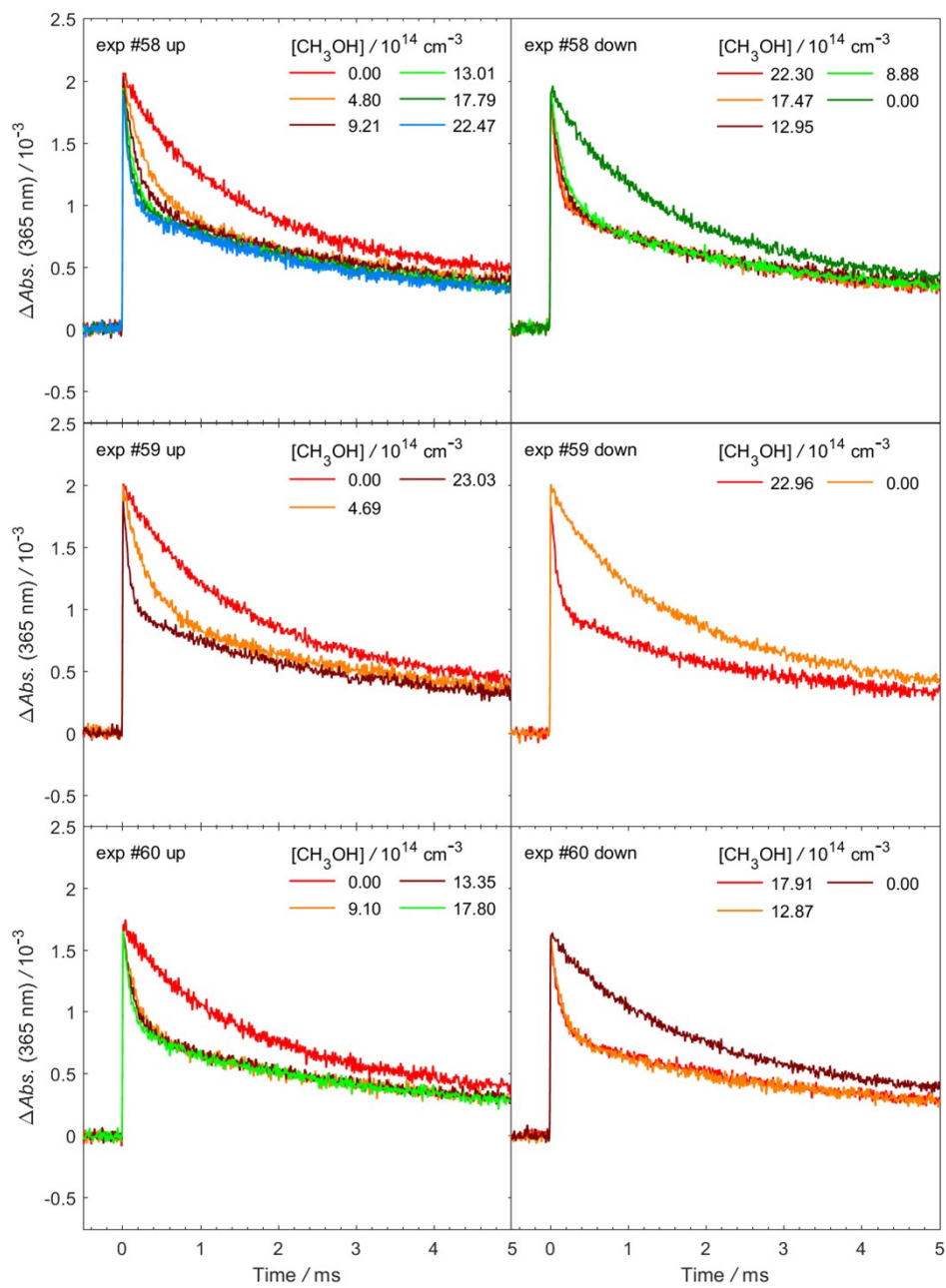| CH₃OH	X	Y	Z
O	-0.7493	0.1219	0.0000
H	-1.1494	-0.7506	0.0000
C	0.6679	-0.0205	0.0000
H	1.0270	-0.5433	-0.8908
H	1.0824	0.9848	0.0000
H	1.0270	-0.5433	0.8908

syn-CH₃CHOO	X	Y	Z
C	-0.6075	-0.6308	-0.1819
O	0.6285	-0.6348	0.0717
H	-1.0046	-1.6231	-0.3575
C	-1.3886	0.6100	-0.2249
H	-2.4312	0.4147	-0.4578
H	-1.2902	1.1287	0.7335
H	-0.9424	1.2890	-0.9577
O	1.2247	0.5731	0.3086

syn-CH₃CHOO+2CH₃OH (2a)	X	Y	Z
C	1.4253	-0.4191	0.0949
H	2.3985	0.0487	-0.0239
O	0.9777	-0.8081	-1.0565
O	-0.2488	-1.5918	-0.9654
O	0.5433	1.1367	0.5274
H	-0.4538	0.8590	0.2561
O	-1.6306	0.3454	-0.3259
H	-1.1451	-0.5522	-0.6767
C	-2.7549	0.0360	0.4853
H	-3.5754	-0.3346	-0.1318
H	-2.5178	-0.7214	1.2387
H	-3.0869	0.9412	0.9936
C	0.9345	2.2201	-0.3278
H	0.9567	1.9025	-1.3711
H	0.2173	3.0310	-0.2136

H	1.9190	2.5651	-0.0183
C	1.1857	-1.1986	1.3452
H	1.6236	-2.1882	1.2030
H	1.6615	-0.7041	2.1878
H	0.1269	-1.3352	1.5336

syn-CH$_3$CHOO+2CH$_3$OH (2b)	X	Y	Z
C	-1.2881	-0.5351	0.5599
H	-1.8438	-0.3011	1.4618
O	-0.3391	-1.3726	0.8265
O	0.3592	-1.8424	-0.3654
O	1.5977	0.2554	-0.5971
H	1.1619	-0.7444	-0.5539
O	-0.4096	1.0958	0.5202
H	0.5301	0.8184	0.0384
C	-0.9960	2.2380	-0.1018
H	-0.3357	3.0924	0.0478
H	-1.1466	2.0876	-1.1718
H	-1.9515	2.4500	0.3762
C	2.8352	0.2953	0.1067
H	2.7383	-0.1173	1.1140
H	3.5907	-0.2759	-0.4344
H	3.1695	1.3303	0.1785
C	-2.0340	-0.5875	-0.7318
H	-2.5089	-1.5693	-0.7844
H	-2.8056	0.1777	-0.7622
H	-1.3666	-0.5034	-1.5822

syn-CH$_3$CHOO+2CH$_3$OH (2c)	X	Y	Z
C	1.4866	-0.3363	-0.2709
H	2.2851	-0.0142	-0.9316
O	0.8717	-1.3529	-0.7843
O	-0.1319	-1.9233	0.1080
O	0.3832	1.0726	-0.6796
H	-0.6117	0.6364	-0.5672
O	-1.7239	-0.1539	-0.4619
H	-1.1341	-1.0397	-0.2030

	X	Y	Z
C	-2.6825	0.1217	0.5482
H	-3.4728	-0.6309	0.5316
H	-2.2354	0.1294	1.5479
H	-3.1342	1.0958	0.3588
C	0.5040	2.3323	-0.0238
H	-0.1984	3.0299	-0.4804
H	0.2960	2.2615	1.0455
H	1.5138	2.7124	-0.1718
C	1.7143	-0.2247	1.2007
H	2.3287	-1.0788	1.4927
H	2.2517	0.6894	1.4406
H	0.7843	-0.2888	1.7540

syn-CH₃CHOO+2CH₃OH (2d)	X	Y	Z
C	1.5087	0.0413	-0.1652
H	2.1839	0.7970	-0.5562
O	0.9285	-0.5816	-1.1426
O	0.1475	-1.7354	-0.7126
O	-1.4667	-0.4754	0.6359
H	-0.8486	-1.1189	0.0131
O	0.2941	1.2454	0.5131
H	-0.5513	0.5918	0.6151
C	-0.0270	2.2573	-0.4481
H	-0.2268	1.8181	-1.4269
H	-0.9061	2.8014	-0.1062
H	0.8117	2.9473	-0.5163
C	-2.7765	-0.3272	0.1050
H	-2.7586	-0.0444	-0.9515
H	-3.3304	-1.2627	0.2020
H	-3.3043	0.4429	0.6682
C	1.9048	-0.6523	1.0962
H	2.5774	-1.4673	0.8240
H	2.4170	0.0444	1.7545
H	1.0494	-1.0873	1.6015

syn-CH₃CHOO+CH₃OH (1a)	X	Y	Z
C	-0.6754	0.5397	-0.6115
H	-0.6593	0.8745	-1.6462
O	-1.4235	-0.4990	-0.4600
O	-1.0168	-1.1676	0.7779
O	0.9563	-0.5225	-0.4948
H	0.3228	-1.0413	0.1960
C	2.1496	-0.0838	0.1433
H	2.8256	-0.9345	0.2462
H	2.6294	0.6693	-0.4803
H	1.9579	0.3329	1.1339
C	-0.4582	1.5622	0.4489
H	0.4442	2.1391	0.2595
H	-1.3063	2.2517	0.3878
H	-0.4380	1.1125	1.4345

syn-CH₃CHOO+CH₃OH (1b)	X	Y	Z
C	-0.6642	-0.3603	0.6332
H	-0.3942	-0.8511	1.5667
O	-0.5881	0.9223	0.7303
O	-0.4958	1.4756	-0.6171
O	0.9188	-0.5429	-0.5164
H	0.5038	0.3664	-0.8589
C	2.1468	-0.2385	0.1497
H	2.5289	-1.1532	0.5981
H	2.8684	0.1348	-0.5775
H	1.9979	0.5218	0.9189
C	-1.5937	-1.0807	-0.2803
H	-1.2357	-2.0905	-0.4626
H	-2.5557	-1.1457	0.2381
H	-1.7266	-0.5455	-1.2127

syn-CH$_3$CHOO+CH$_3$OH (1c)	X	Y	Z
C	1.3672	0.4674	0.5617
O	1.2208	-0.8124	0.5430
O	0.5737	-1.3398	-0.6241
H	1.7788	0.7842	1.5160
O	-1.3323	0.1594	-0.5863
H	-0.5620	-0.6523	-0.6187
C	0.9300	1.3628	-0.4181
H	-0.3639	1.0305	-0.4231
H	1.1816	2.3992	-0.2416
H	1.0502	1.0152	-1.4421
C	-2.2073	0.0524	0.5346
H	-3.1134	0.6226	0.3363
H	-2.4722	-0.9915	0.6988
H	-1.7360	0.4393	1.4442

syn-CH$_3$CHOO+CH$_3$OH (1d)	X	Y	Z
C	-1.6212	0.5377	-0.2349
O	-1.5844	-0.7500	-0.2369
O	-0.4925	-1.3323	0.4866
H	-2.4096	0.8911	-0.8933
O	1.2337	0.0050	-0.5778
H	0.5417	-0.7420	-0.1048
C	-0.7066	1.3904	0.3883
H	0.4064	0.9491	-0.2268
H	-0.9351	2.4443	0.3105
H	-0.3637	1.0528	1.3639
C	2.4968	0.0474	0.0846
H	3.0031	-0.9098	-0.0365
H	3.1075	0.8267	-0.3677
H	2.3824	0.2535	1.1526

anti-CH₃CHOO+CH₃OH (a)	X	Y	Z
C	-0.7438	-0.2555	0.3539
H	-0.2213	-0.1886	1.3030
O	-1.1841	0.8377	-0.1481
O	-0.1856	1.8665	0.1215
O	0.9984	-0.1420	-0.5618
H	0.7688	0.8891	-0.3684
C	2.1402	-0.5292	0.1910
H	2.0253	-0.2941	1.2538
H	2.2927	-1.6010	0.0735
H	3.0209	-0.0046	-0.1829
C	-1.4202	-1.5151	-0.0436
H	-0.7213	-2.3460	0.0288
H	-2.2446	-1.7098	0.6469
H	-1.8075	-1.4445	-1.0561

anti-CH₃CHOO+CH₃OH (b)	X	Y	Z
C	0.8942	-0.0196	0.3475
H	0.9361	0.2996	1.3820
O	0.7516	0.8931	-0.5443
O	-0.1568	1.8892	0.0127
O	-1.0265	-0.2844	0.6865
H	-0.9529	0.7688	0.4978
C	-1.7443	-0.8772	-0.3947
H	-1.7187	-1.9593	-0.2791
H	-2.7815	-0.5403	-0.3672
H	-1.3139	-0.5963	-1.3587
C	1.5396	-1.2918	-0.0631
H	2.6182	-1.2034	0.0873
H	1.1825	-2.1024	0.5692
H	1.3468	-1.5171	-1.1088

Reference

1. S. P. Sander, J. R. Barker, D. M. Golden, M. J. Kurylo, P. H. Wine, J. P. D. Abbatt, J. B. Burkholder, C. E. Kolb, G. K. Moortgat, R. E. Huie and V. L. Orkin, *JPL Publ.*, 2011, **10–6**.

2. M. C. Smith, W.-L. Ting, C.-H. Chang, K. Takahashi, K. A. Kristie A. Boering and J. J. Lin, *J. Chem. Phys.*, 2014, **141**, 074302.

3. B.-M. Cheng, M. Bahou, Y.-P. Lee and L. C. Lee, *J. Geophys. Res. Space Physics.*, 2002, **107 (A8)**, SIA 7-1–SIA 7-5.

4. L.-C.Lin, W. Chao, C. -H.Chang, K. Takahashi and J. J. L in, *Phys. Chem. Chem. Phys.*, 2016, **18**, 28189–28197.

5. Y.-H. Lin, K. Takahashi and J. J. Lin, *J. Phys. Chem. Lett.*, 2018, **9**, 184–188.

6. D. L. Osborn, and C. A. Taatjes, *Int. Rev. Phys. Chem.*, 2015, **34:3**, 309–360

7. A. M. Green, V. P. Barber, Y. Fang, S. J. Klippenstein and M. I. Lester, *Proc. Natl. Acad. Sci.U. S. A.*, 2017, **114**, 12372–12377.

8. M. C. Smith, W. Chao, K. Takahashi, K. A. Boering, and J. J. Lin, *J. Phys. Chem. A*, 2016, **120**, 4789-4798.

9. R. Renaud, and L. *C. Leitch, Can. J. Chem.*, 1954, **32**, 545